J|A|C|S
ARTICLES
Published on Web 05/27/2007

Transition Metal−Carbon Complexes. A Theoretical Study§

Andreas Krapp,*,‡ Krishna K. Pandey,*,† and Gernot Frenking*,‡

Contribution from the School of Chemical Sciences, Devi Ahilya University Indore, Indore-452017, India, and the Fachbereich Chemie, Philipps-Universität Marburg, D-35032 Marburg, Germany

Received December 20, 2006; E-mail: frenking@chemie.uni-marburg.de

Abstract: The equilibrium geometries and bond dissociation energies of 16VE and 18VE complexes of ruthenium and iron with a naked carbon ligand are reported using density functional theory at the BP86/TZ2P level. Bond energies were also calculated at CCSD(T) using TZ2P quality basis sets. The calculations of $[Cl_2(PMe_3)_2Ru(C)]$ (**1Ru**), $[Cl_2(PMe_3)_2Fe(C)]$ (**1Fe**), $[(CO)_2(PMe_3)_2Ru(C)]$ (**2Ru**), $[(CO)_2(PMe_3)_2Fe(C)]$ (**2Fe**), $[(CO)_4Ru(C)]$ (**3Ru**), and $[(CO)_4Fe(C)]$ (**3Fe**) show that **1Ru** has a very strong Ru−C bond which is stronger than the Fe−C bond in **1Fe**. The metal−carbon bonds in the 18VE complexes **2Ru**−**3Fe** are weaker than those in the 16VE species. Calculations of the related carbonyl complexes $[(PMe_3)_2Cl_2Ru(CO)]$ (**4Ru**), $[(PMe_3)_2Cl_2Fe(CO)]$ (**4Fe**), $[(PMe_3)_2Ru(CO)_3]$ (**5Ru**), $[(PMe_3)_2Fe(CO)_3]$ (**5Fe**), $[Ru(CO)_5]$ (**6Ru**), and $[Fe(CO)_5]$ (**6Fe**) show that the metal−CO bonds are much weaker than the metal−C bonds. The 18VE iron complexes have a larger BDE than the 18VE ruthenium complexes, while the opposite trend is calculated for the 16VE compounds. Charge and energy decomposition analyses (EDA) have been carried out for the calculated compounds. The Ru−C and Fe−C bonds in **1Ru** and **1Fe** are best described in terms of two electron-sharing bonds with σ and π symmetry and one donor−acceptor π bond. The bonding situation in the 18 VE complexes **2Ru**−**3Fe** is better described in terms of closed shell donor−acceptor interactions in accordance with the Dewar−Chatt−Duncanson model. The bonding analysis clearly shows that the 16VE carbon complexes **1Ru** and **1Fe** are much more strongly stabilized by metal−C σ interactions than the 18VE complexes which is probably the reason why the substituted homologue of **1Ru** could become isolated. The EDA calculations show that the nature of the TM−C and TM−CO binding interactions resembles each other. The absolute values for the energy terms which contribute to ΔE_{int} are much larger for the carbon complexes than for the carbonyl complexes, but the relative strengths of the energy terms are not very different from each other. The π bonding contribution to the orbital interactions in the carbon complexes is always stronger than σ bonding. There is no particular bonding component which is responsible for the reversal of the relative bond dissociation energies of the Ru and Fe complexes when one goes from the 16VE complexes to the 18VE species. That the 18 VE compounds have longer and weaker TM−C and TM−CO bonds than the respective 16 VE compounds holds for all complexes. This is because the LUMO in the 16 VE species is a σ-antibonding orbital which becomes occupied in the 18 VE species.

Introduction

Transition metal (TM) complexes with a terminal carbon atom as ligand can be regarded as the endpoint in the series TM−alkyl (TM−CR_3) → TM−carbene (TM=CR_2) → TM−carbyne (TM≡CR) complexes. Alkyl complexes of transition metals are already known since 1848 when Frankland reported about the accidental synthesis of diethylzinc while attempting to prepare free ethyl radicals.[1] Molecules with a TM=CR_2 double bond and TM≡CR triple bond were synthesized much later.[2−5] Experimental studies have shown that there are two discriminative classes of carbene and carbyne complexes which exhibit different reactivities. The metal−ligand bonding in Fischer-type carbene and carbyne complexes[2,3] is best described in terms of donor−acceptor bonding between closed-shell fragments, while the bonding in Schrock carbenes and carbynes[4,5] should be considered as electron-sharing interactions between triplet (for carbenes) and quartet (for carbynes) fragments (Figure 1).[6−9]

The final member in the above series of metal−carbon bonds has a naked carbon atom as ligand. The first TM complex with a singly coordinated carbon atom[10] was synthesized by Cummins and co-workers in 1997.[11] They fully characterized the 14 valence electron (VE) anion $[(NRAr)_3Mo(C)]^-$ (R = $C(CD_3)_2$-

† Devi Ahilya University Indore.
‡ Philipps-Universität Marburg.
§ Theoretical Studies of Organometallic Compounds. 56. Part 55: Fernández, I.; Frenking, G. *Chem.*−*Eur. J.* ASAP.

(1) Elschenbroich, C. *Organometallics*, 2nd ed.; VCH: Weinheim, 1992.
(2) Fischer, E. O.; Kreis, G.; Kreiter, C. G.; Müller, J.; Huttner, G.; Lorenz, H. *Angew. Chem, Int. Ed. Engl.* **1973**, *12*, 564; *Angew. Chem.* **1973**, *85*, 618.
(3) Fischer, E. O.; Maasböl, A. *Angew. Chem.* **1964**, *76*, 645.
(4) McLain, S. J.; Wood, C. D.; Messerle, L. W.; Schrock, R. R.; Hollander, F. J.; Youngs, W. J.; Churchill, M. R. *J. Am. Chem. Soc.* **1978**, *100*, 5962.
(5) Schrock, R. R. *J. Am. Chem. Soc.* **1974**, *96*, 6796.
(6) Frenking, G.; Sola, M.; Vyboishchikov, S. F. *J. Organomet. Chem.* **2005**, *690*, 6178.
(7) Frenking, G.; Fröhlich, N. *Chem. Rev.* **2000**, *100*, 717.
(8) Vyboishchikov, S. F.; Frenking, G. *Chem.*−*Eur. J.* **1998**, *4*, 1428.
(9) Vyboishchikov, S. F.; Frenking, G. *Chem.*−*Eur. J.* **1998**, *4*, 1439.
(10) Bruce, M. I.; Low, P. J. *Adv. Organomet. Chem.* **2004**, *50*, 179.
(11) Peters, J. C.; Odom, A. L.; Cummins, C. C. *Chem. Commun.* **1997**, 1995.

10.1021/ja0691324 CCC: $37.00

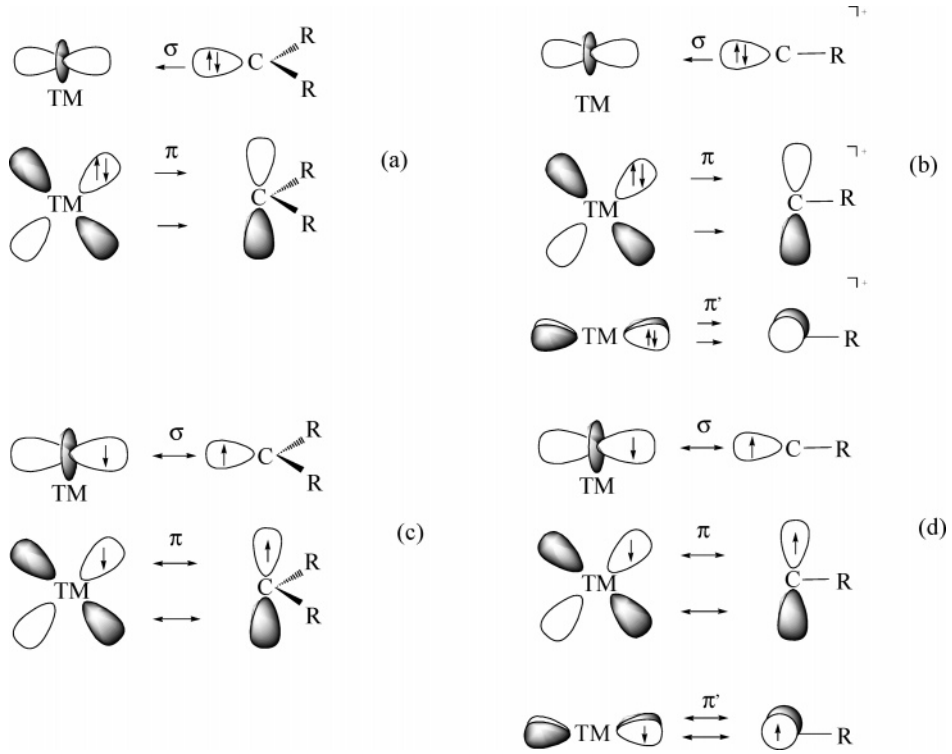

Figure 1. Pictorial representation of the bonding situation in (a) Fischer-type carbene complexes; (b) Fischer-type carbyne complexes; (c) Schrock-type carbenes (alkylidenes); (d) Schrock-type carbynes (alkylidynes).

CH_3, Ar = $C_6H_3Me_2$-3,5) which is isoelectronic with the previously known nitrido complex $[(NRAr)_3Mo(N)]$.[12,13] The bonding situation in the carbon compounds is very similar to the nitrogen homologues which indicates that the former species are best described as metal carbides which have a TM≡C^- electron-sharing triple bond. The compounds may also be viewed as the anion of Schrock-type carbynes [TM]≡CR where the positively charged substituent R^+ has dissociated. The bonding model for Schrock carbynes (Figure 1d) may therefore be used for the metal−carbon bonding in the carbide.

Shortly after the experimental work by Cummins about negatively charged carbides appeared, we reported about a theoretical study which addressed the question if neutral complexes with terminal carbon atoms as ligands may become synthesized.[14] Such carbon complexes were not known at that time. We calculated the neutral TM complex $[(CO)_4Fe(C)]$ and the related carbene and carbyne compounds $[(CO)_4Fe(CH_2)]$ and $[I(CO)_3Fe(CH)]$. A charge decomposition analysis of the bonding situation showed that the singly coordinated carbon atom in the 18 valence electron (18VE) complex $[(CO)_4Fe(C)]$ is a strong σ donor but also a strong π acceptor. This comes from the electronic reference state of the bonded carbon atom in the complex which has the configuration $(2s)^2(2p_{z(\sigma)})^2(2p_{x(\pi)})^0(2p_{y(\pi)})^0$.[14] The compound $[(CO)_4Fe(C)]$ should therefore be termed carbon complex rather than carbide. The calculations at the CCSD(T) level of theory predicted that the bond dissociation energy of the $(CO)_4Fe-C$ bond is rather large (D_e = 94.5 kcal/mol).[14] $[(CO)_4Fe(C)]$ has been suggested[15] as intermediate in the reaction of $[(CO)_4Fe(CS)]$ with $P(NMe_2)_3$, but it seems highly unlikely that it can be isolated in a condensed phase. Fischer carbene complexes [TM]=CR_2 can only become isolated when at least one π-donor substituent R stabilizes the formally vacant p(π) carbon orbital (Figure 1a). The ligand atom in carbon complexes has even two vacant p(π) carbon orbitals.

The first synthesis and X-ray structure analysis of a neutral transition metal compound with a terminal carbon ligand was recently reported by Heppert and co-workers.[16] They isolated the diamagnetic 16VE ruthenium complexes $[(PCy_3)LCl_2Ru(C)]$ (**I**: L = PCy_3; **II**: L = 1,3-dimesityl-4,5-dihydroimidazol-2-ylidene; Cy = Cyclohexyl) by a metathesis facilitated reaction. Shortly later, Grubbs and his group showed that **I** can act as a σ-donor toward $Mo(CO)_5$ and $Pd(SMe_2)Cl_2$ via the terminal carbon atom.[17] In 2005 Johnson and co-workers reported about two new generalizable routes to the air- and moisture-stable $[(PCy_3)_2Cl_2Ru(C)]$, opening the way for broader research on the chemistry of complexes with terminal C.[18] The same group recently published the results of further experimental studies which show that $[(PCy_3)_2Cl_2Ru(C)]$ reacts with $MeO_2CC{\equiv}CCO_2Me$ in a formal [1 + 2] cycloaddition of the carbon ligand yielding the cyclopropenylidene complex $[(PCy_3)_2Cl_2Ru{=}CC_2(CO_2Me)_2]$.[19]

The synthesis of **I** and **II** raises the question about the metal−carbon bonding situation in the compounds. Heppert et al. noted[16] that the Ru−C distance in **II** is 0.15 Å shorter than that in typical carbene complexes and that it resembles a triple bond more while the Ru−P and Ru−Cl bonds are nearly identical to

(12) Laplaza, C. E.; Odom, A. L.; Davis, W. M.; Cummins, C. C.; Protasiewicz, J. D. *J. Am. Chem. Soc.* **1995**, *117*, 861.
(13) Laplaza, C. E.; Cummins, C. C. *Science* **1995**, *268*, 861.
(14) Chen, Y.; Petz, W.; Frenking, G. *Organometallics* **2000**, *19*, 2698.
(15) Petz, W.; Weller, F. *Organometallics* **1993**, *12*, 4056.
(16) Carlson, R. G.; Gile, M. A.; Heppert, J. A.; Mason, M. H.; Powell, D. R.; Velde, D. V.; Vilain, J. M. *J. Am. Chem. Soc.* **2002**, *124*, 1580.
(17) Hejl, A.; Trnka, T. M.; Day, M. W.; Grubbs, R. H. *Chem. Commun.* **2002**, 2524.
(18) Caskey, S. R.; Stewart, M. H.; Kivela, J. E.; Sootsman, J. R.; Johnson, M. J. A.; Kampf, J. W. *J. Am. Chem. Soc.* **2005**, *127*, 16750.
(19) Caskey, S. R.; Stewart, M. H.; Johnson, M. J. A.; Kampf, J. W. *Angew. Chem, Int. Ed.* **2006**, *45*, 7422; *Angew. Chem.* **2006**, *118*, 7582.

analogous bonds in ruthenium carbene complexes. This indicates that the electronic structure in the ruthenium moiety to which the carbon atom is bonded is similar to that in carbene complexes, and thus, **I** and **II** might be considered as the first examples of stable carbon complexes. The question remains why can the 16 VE complexes **I** and **II** become isolated as stable complexes while the 18 VE complex [$(CO)_4Fe(C)$] is apparently not stable. What is the nature of the metal−carbon bonding in the 16 and 18 VE complexes? Which factor is responsible for the stability of the electron deficient 16 VE carbon complex? What is the influence of the different substituents and the metal atom on the bonding situation and the stability of the complexes?

In order to address the above questions we first calculated the geometries and bond dissociation energies of the 16 VE carbon complexes [$(PMe_3)_2Cl_2Ru(C)$] (**1Ru**) and [$(PMe_3)_2Cl_2$-$Fe(C)$] (**1Fe**) using density functional theory (BP86/TZ2P). Our work is the first theoretical study of the newly synthesized class of carbon complexes. The complex **1Ru** shall be used as a model compound for **I**. We also theoretically studied the 18VE carbon complexes [$(PMe_3)_2(CO)_2Ru(C)$] (**2Ru**), [$(PMe_3)_2(CO)_2Fe(C)$] (**2Fe**), [$(CO)_4Ru(C)$] (**3Ru**), and [$(CO)_4Fe(C)$] (**3Fe**). In order to compare the carbon complexes with CO complexes we also calculated the compounds [$(PMe_3)_2Cl_2Ru(CO)$] (**4Ru**), [$(PMe_3)_2$-$Cl_2Fe(CO)$] (**4Fe**), [$(PMe_3)_2Ru(CO)_3$] (**5Ru**), [$(PMe_3)_2Fe(CO)_3$] (**5Fe**), [$Ru(CO)_5$] (**6Ru**), and [$Fe(CO)_5$] (**6Fe**). The bonding situation in the molecules was investigated with the energy decomposion analysis (EDA)[20] which has previously been used by us in systematic studies of transition metal complexes.[21−23] The EDA makes it possible to quantitatively estimate the contributions of orbitals which possess different symmetry to the overall metal−ligand orbital interactions. The molecules **1Ru**−**6Fe** and the fragments which are used for the EDA have at least C_{2v} symmetry which is very helpful because the contributions of the $a_1(\sigma)$, $a_2(\delta)$, $b_1(\pi_{II})$, and $b_2(\pi_{\perp})$ orbitals can be distinguished. A short description of the EDA method is given in the method section. We also used the NBO[24] method for the analysis of the electronic structure. Improved energy calculations were carried out using coupled-cluster theory[25] at the CCSD(T) level.[26−30]

Computational Details

The geometries of all complexes have been optimized at the gradient corrected DFT level of theory using the exchange functional of Becke[31] in conjunction with the correlation functional of Perdew[32,33] (BP86). Uncontracted Slater-type orbitals (STOs) were employed as basis functions for the SCF calculations.[34] The basis sets have triple ζ-quality augmented by two sets of polarization functions. The $(n-1)s^2$ and the $(n-1)p^6$ core electrons of the main group elements and the $(1s2s2p)^{10}$ core electrons of iron and the $(1s2s2p3s3p3d)^{28}$ core electrons of ruthenium were treated by the frozen core approximation.[35] This level of theory is denoted as BP86/TZ2P. An auxiliary set of s, p, d, f, and g STOs was used to fit the molecular densities and to represent the Coulomb and exchange potentials accurately in each SCF cycle.[36] Scalar relativistic effects have been considered using the zero-order regular approximation (ZORA).[37−41] The nature of the stationary points on the potential energy surface has been verified by calculating the Hessian matrices.[42,43] Some species have very small imaginary modes ($<i20$ cm^{-1}) which correspond in all cases to ligand rotations. We followed these modes for a number of cases by lifting the symmetry constrains and noticed only minor effects on the geometries and energies. Therefore these small modes will be listed in the figures but will be neglected in the following discussions. The calculations were carried out with the program package ADF.2004 and ADF.2005.[44−46]

The bonding interactions between two molecular fragments A and B forming a molecule AB have been analyzed with the energy decomposition scheme of the program package ADF,[20] which is based on the work by Morokuma[47,48] and Ziegler and Rauk.[49] The bond dissociation energy ($-\Delta E$ = BDE) between the fragments A and B is partitioned into several contributions which can be identified as physically meaningful quantities. First, ΔE is separated into two major components ΔE_{int} and ΔE_{prep}:

$$\Delta E\ (= -\mathrm{BDE}) = \Delta E_{int} + \Delta E_{prep}$$

ΔE_{prep} is the energy which is necessary to promote the fragments A and B from their equilibrium geometry and electronic ground state to the geometry and electronic state which they have in the molecule. The instantaneous interaction energy ΔE_{int} is the focus of the bonding analysis and can be decomposed into three components:

$$\Delta E_{int} = \Delta E_{elstat} + \Delta E_{Pauli} + \Delta E_{orb}$$

The term ΔE_{elstat} gives the electrostatic interaction energy between the fragments which are calculated with a frozen density distribution in the geometry of the complex. The Pauli repulsion (ΔE_{Pauli}) arises as the energy change associated with the transformation from the superposition of the unperturbed electron densities of fragments $\rho_A + \rho_B$ to the wavefunction $\Psi^0 = N\hat{A}\{\Psi_A \bullet \Psi_B\}$, which properly obeys the Pauli principle through explicit antisymmetrization ($\hat{A}$) and renormalization (N) of the product wavefunction. It comprises the destabilizing interactions between electrons on either fragment with the same spin. The stabilizing orbital interaction term ΔE_{orb} is calculated in the final step of the analysis when the orbitals relax to their final form. The

(20) Bickelhaupt, F. M.; Baerends, E. J. In *Reviews in Computational Chemistry*; Lipkowitz, K. B., Boyd, D. B., Eds.; Wiley-VCH: New York, 2000; Vol. 15, p 1.
(21) Frenking, G.; Wichmann, K.; Fröhlich, N.; Loschen, C.; Lein, M.; Frunzke, J.; Rayon, V. M. *Coord. Chem. Rev.* **2003**, *238*−*239*, 55.
(22) Lein, M.; Szabo, A.; Kovacs, A.; Frenking, G. *Faraday Discuss.* **2003**, *124*, 365.
(23) Lein, M.; Frenking, G. In *Theory and Applications of Computational Chemistry: The First 40 Years*; Dykstra, C. E., Frenking, G., Kim, K. S., Scuseria, G. E., Eds.; Elsevier: Amsterdam, 2005; p 291.
(24) Reed, A. E.; Curtiss, L. A.; Weinhold, F. *Chem. Rev.* **1988**, *88*, 899.
(25) Cizek, J. *J. Chem. Phys.* **1966**, *45*, 4256.
(26) Bartlett, R. J.; Purvis, G. D. *Int. J. Quantum Chem.* **1978**, *14*, 516.
(27) Pople, J. A.; Krishnan, R.; Schlegel, H. B.; Binkley, J. S. *Int. J. Quantum Chem.* **1978**, *14*, 545.
(28) Purvis, G. D.; Bartlett, R. J. *J. Chem. Phys.* **1982**, *76*, 1910.
(29) Hampel, C.; Peterson, K.; Werner, H.-J. *Chem. Phys. Lett.* **1992**, *190*, 1.
(30) Pople, J. A.; Head-Gordon, M.; Raghavachari, K. *J. Chem. Phys.* **1987**, *87*, 5968.
(31) Becke, A. D. *Phys. Rev. A* **1988**, *38*, 3098.
(32) Perdew, J. P. *Phys. Rev. B* **1986**, *34*, 7406.
(33) Perdew, J. P. *Phys. Rev. B* **1986**, *33*, 8822.
(34) Snijders, J. G.; Baerends, E. J. *A. Data Nucl. Data Tables* **1982**, *26*, 483.
(35) Baerends, E. J.; Ellis, D. E.; Ros, P. *J. Chem. Phys.* **1973**, 41.
(36) Krijn, J.; Baerends, E. J. *Fit Functions in the HFS-Method, Internal Report (in Dutch)*; Vrije Universiteit: Amsterdam, the Netherlands, 1984.
(37) Chang, C.; Pelissier, M.; Durand, P. *Phys. Scr.* **1986**, *34*, 394.
(38) Heully, J.-L.; Lindgren, I.; Lindroth, E.; Lundquist, S.; Martensson-Pendrill, A.-M. *J. Phys. B* **1986**, *19*, 2799.
(39) van Lenthe, E.; Baerends, E. J.; Snijders, J. G. *J. Chem. Phys.* **1993**, *99*, 4597.
(40) van Lenthe, E.; van Leeuwen, R.; Baerends, E. J.; Snijders, J. G. *Int. J. Quantum Chem.* **1996**, *57*, 281.
(41) van Lenthe, J. G.; Baerends, E. J.; Snijders, J. G. *J. Chem. Phys.* **1996**, *105*, 6505.
(42) Fan, L.; Ziegler, T. *J. Chem. Phys.* **1992**, *96*, 9005.
(43) Fan, L.; Ziegler, T. *J. Phys. Chem.* **1992**, *96*, 6937.
(44) Fonseca, Guerra, C.; Snijders, J. G.; Te, Velde, G.; Baerends, E. J. *Theor. Chem. Acc.* **1998**, *99*, 1998.
(45) *ADF2004.01* and *ADF2005.01*; Theoretical Chemistry, Vrije Universiteit, SCM, http://www.scm.com; Amsterdam, The Netherlands
(46) Te, Velde, G.; Bickelhaupt, F. M.; Baerends, E. J.; Fonseca, Guerra, C.; Van, Gisbergen, S. J. A.; Snijders, J. G.; Ziegler, T. *J. Comput. Chem.* **2001**, *22*, 931.
(47) Morokuma, K. *J. Chem. Phys.* **1971**, *55*, 1236.
(48) Kitaura, K.; Morokuma, K. *Int. J. Quantum Chem.* **1976**, *10*, 325.
(49) Ziegler, T.; Rauk, A. *Theor. Chem. Acta* **1977**, *46*, 1.

latter can be decomposed into contributions from each irreducible representation of the point group of the interacting system.

In order to perform the NBO analysis[24,50] of our model complexes we made single-point calculations at BP86/TZ2P optimized geometries with the Gaussian03[51] program using the BP86 functional and a basis set of triple-ζ quality with two polarization functions (def2-TZVPP).[52]

Improved energy calculations at the BP86/TZ2P optimized geometries have been carried out using coupled-cluster theory at the CCSD(T)[26−30] level in combination with the basis sets of triple-ζ quality for the main group atoms from Dunning (cc-pVTZ) as delivered in the Molpro basis set library.[53] For iron and ruthenium we used small core relativistic ECPs in combination with the [6s5p3d] basis sets[54,55] augmented by two sets of f-functions and a set of g-functions.[56] This level will be denoted as CCSD(T)/BS1. For the CCSD(T) calculations we used the Molpro program.[53]

For the complexes **1**−**6** we optimized the geometries on the singlet, triplet, and quintet potential energy surface and found in all cases the triplet and quintet states to be higher in energy. Therefore in the discussion of these complexes only singlet states will be considered. Whenever we mention a value without explicitly giving the level of theory we discuss BP86/TZ2P values. All calculations have been carried out on the Dual-Opteron Linux-PC-cluster "MaRC" in Marburg and on the IBM machines of the HHLR in Darmstadt.

Geometries and Bond Energies

Figure 2 shows the optimized geometries at BP86/TZ2P of the complexes **1Ru**−**6Fe** and the fragments **7**−**9** which are formed after dissociation of the ligands C or CO from the former complexes. The metal fragments have been calculated at the lowest singlet and triplet electronic states. Experimental values of related complexes are also given.

The 16VE model compound $[Cl_2(PMe_3)_2Ru(C)]$ (**1Ru**) has a C_{2v} trigonal bipyramidal geometry with the carbon ligand and the chlorine atoms in the equatorial positions. The metal−carbon bond distance of 1.661 Å in **1Ru** is slightly longer than the experimentally determined Ru−C distances of 1.632(6) Å in $[Cl_2(PCy_3)_2Ru(C)]$ (**I**)[17] and 1.650(2) Å in $[Cl_2(PCy_3)$(1,3-dimesityl-4,5-dihydroimidazol-2-ylidene)RuC] (**II**).[16] The calculated Cl−Ru−Cl bond angle in the model compound **1Ru** is more acute (138.5°) than the experimental values for **I** and **II** (156.7° and 156.9°) which could be caused by the larger phosphine groups in the latter species. The calculated P−Ru−P angle in **1Ru** (167.0°) is in good agreement with the experimental value for **I** (169.3°), while the value for **II** is somewhat smaller (160.7°). The calculated iron−carbon bond of the isostructural iron analogue $[Cl_2(PMe_3)_2Fe(C)]$ (**1Fe**) is also rather short (1.548 Å).

The 18VE complexes $[(CO)_2(PMe_3)_2Ru(C)]$ (**2Ru**) and $[(CO)_2(PMe_3)_2Fe(C)]$ (**2Fe**) also have a C_{2v} symmetric trigonal bipyramidal geometry with the terminal carbon atom and the carbonyl groups occupying the equatorial positions (see Figure 2). The metal−carbon bonds in **2Ru** (1.748 Å) and **2Fe** (1.642 Å) are significantly longer than those in the 16VE complexes **1Ru** and **1Fe**, while the TM−P distances change slightly. The calculated bond angles exhibit interesting differences between the 16VE and 18VE complexes. The PR_3 ligands in **2Ru** and **2Fe** are slightly tilted toward the carbon ligand, while in **1Ru** and **1Fe** they are tilted away from the C atom. The bond angles OC−TM−CO between the carbonyl ligands in **2Ru** (115.6°) and **2Fe** (112.9°) are much more acute than the Cl−TM−Cl angles in **1Ru** and **1Fe**.

The geometry optimization of the tetracarbonyl complexes $[(CO)_4Ru(C)]$ (**3Ru-eq**) and $[(CO)_4Fe(C)]$ (**3Fe-eq**) where the carbon ligand is in the equatorial position yields stationary points on the PES which have one imaginary mode ($i = 1$); i.e., they are transition states. This is in agreement with our previous study of **3Fe**.[14] The calculation of the isomeric forms **3Ru-ax** and **3Fe-ax** where the carbon ligand is in the axial position gives energy minima ($i = 0$) which are at BP86/TZ2P 5.2 kcal/mol (**3Ru**) and 6.6 kcal/mol (**3Fe**) lower lying than the equatorial forms. Energy calculations at CCSD(T)/BS1 support the DFT results (Figure 2). The energy differences at the ab initio level amount to 12.2 kcal/mol and 7.1 kcal/mol for **3Ru** and **3Fe**, respectively. Please note that the axial TM−CO bonds which are *trans* to the carbon ligand in **3Ru-ax** and **3Fe-ax** are much longer than the equatorial TM−CO bonds. This holds particularly for the ruthenium complex **3Ru-ax** where the calculated Ru−CO distance of 2.477 Å indicates that the carbonyl ligand has nearly dissociated. The latter compound does not appear to be stable enough to become isolated in a condensed phase, but the electronically unsaturated species $[(CO)_3Ru(C)]$ might be an observable species.

Figure 2 gives also the optimized geometries of the carbonyl complexes **4Ru**−**6Fe** which are in good agreement with experimental values. The calculated bond lengths and bond angles of **4Ru**−**6Fe** shall be compared with the analogue carbon complexes **1Ru**−**3Fe**. There is a small but consistent change in the axial metal−ligand bond lengths. The axial TM−PMe_3 and TM−CO bonds of the carbon complexes [TM]−C which have C in an equatorial position are always longer than the axial bonds of the respective carbonyl complex [TM]−CO. For example, the Ru−PMe_3 distance elongates from 2.375 Å in **4Ru** to 2.394 Å in **1Ru**, while the Fe−PMe_3 distance increases from 2.264 Å in **4Fe** to 2.271 Å in **1Fe**. The TM−CO_{ax} distance increases likewise. The Ru−CO_{ax} distance elongates from 1.953 Å in **6Ru** to 1.997 Å in **3Ru-eq** while the Fe−CO_{ax} distance increases from 1.803 Å in **6Fe** to 1.828 Å in **3Fe-eq**. A larger change is found for the equatorial bond lengths where the substitution of CO by C yields significantly longer TM−Cl and TM−CO_{eq} distances particularly for the ruthenium complexes. The Ru−Cl bond length in **4Ru** (2.276 Å) elongates to 2.389 Å in **1Ru**, and the Fe−Cl distance increases from 2.237 Å in **4Fe** to 2.252 Å in **1Fe**. The Ru−CO_{eq} distance elongates from 1.953 Å in **6Ru** to 2.022 Å in **3Ru-eq**, while the Fe−CO_{eq} distance increases from 1.801 Å in **6Fe** to 1.846 Å in **3Fe-eq**. The changes in the bond lengths suggest that the substitution of the equatorial CO ligand in **4Ru**−**6Fe** by a carbon ligand weakens the axial but particularly the other equatorial metal−ligand bonds.

The metal fragments **8Ru** and **8Fe** deserve special attention because a homologue of the electronically unsaturated 16 VE complex $\mathbf{8Ru^S}$ where the PMe_3 ligand is substituted by the more bulky phosphane group P^tBu_2Me in $[(CO)_2(P^tBu_2Me)_2Ru]$ has been isolated and characterized by X-ray structure analysis by

(50) Glendening, E. D.; Reed, A. E.; Carpenter, J. E.; Weinhold, F. *NBO*, version 3.1.
(51) Frisch, M. J., et al. *Gaussian 03*, revision D.01; Gaussian Inc.: Wallingford, CT, 2004.
(52) Weigend, F.; Ahlrichs, R. *Phys. Chem. Chem. Phys.* **2005**, *7*, 3297.
(53) Werner, H.-J., et al. *MOLPRO, a package of ab initio programs*, version 2006.1. See http://www.molpro.net.
(54) Andrae, D.; Haeussermann, U.; Dolg, M.; Stoll, H.; Preuss, H. *Theor. Chim. Acta* **1990**, *77*, 123.
(55) Dolg, M.; Wedig, U.; Stoll, H.; Preuss, H. *J. Chem. Phys.* **1987**, *86*, 866.
(56) Martin, J. M. L.; Sundermann, A. *J. Chem. Phys.* **2001**, *114*, 3408.

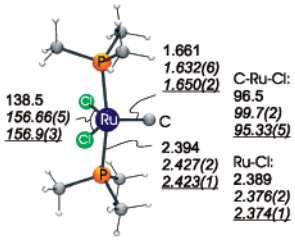

1Ru

C_{2v}; $^1A_1$; NImag=0
exp.val.:**a**
exp.val.:**b**

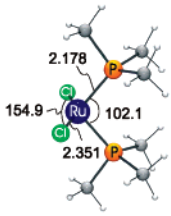

7Ru^S

C_{2v}; $^1A_1$
NImag=1 (i19cm^{-1})
E_{rel}=0.0 kcal•mol^{-1}

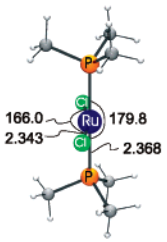

7Ru^T

C_{2v}; $^3B_1$
NImag=2 (2xi21cm^{-1})
E_{rel}=15.0 kcal•mol^{-1}

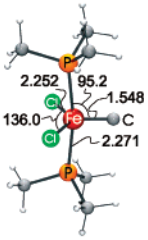

1Fe

C_{2v}; $^1A_1$
NImag=0

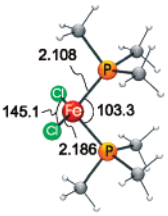

7Fe^S

C_{2v}; $^1A_1$
NImag=0
E_{rel}=4.6 kcal•mol^{-1}

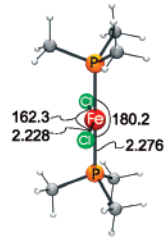

7Fe^T

C_{2v}; $^3B_1$
NImag=1 (i16cm^{-1})
E_{rel}=0.0 kcal•mol^{-1}

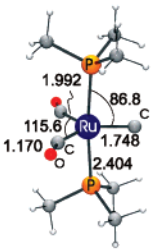

2Ru

C_{2v}; $^1A_1$
NImag=0

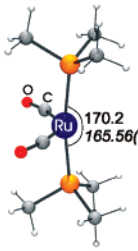

Ru-P:
2.341
2.3596(22)/
2.3542(22)
Ru-C:
1.877
1.886(10)/
1.854(9)
C-O:
1.178
1.153(11)/
1.177(10)
C-Ru-C:
132.2
133.3(4)

8Ru^S

C_{2v}; $^1A_1$; NImag=0
E_{rel}=0.0 kcal•mol^{-1}
exp.val. **c**

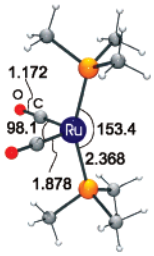

8Ru^T

C_{2v}; $^3B_1$; NImag=0
E_{rel}=18.3 kcal•mol^{-1}

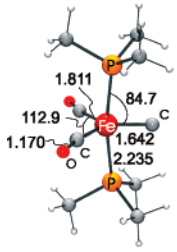

2Fe

C_{2v}; $^1A_1$
NImag=0

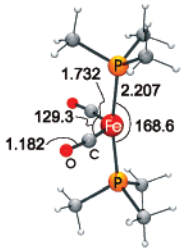

8Fe^S

C_{2v}; $^1A_1$
NImag=0
E_{rel}=0.0 kcal•mol^{-1}

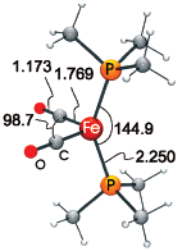

8Fe^T

C_{2v}; $^3B_1$
NImag=0
E_{rel}=0.9 kcal•mol^{-1}

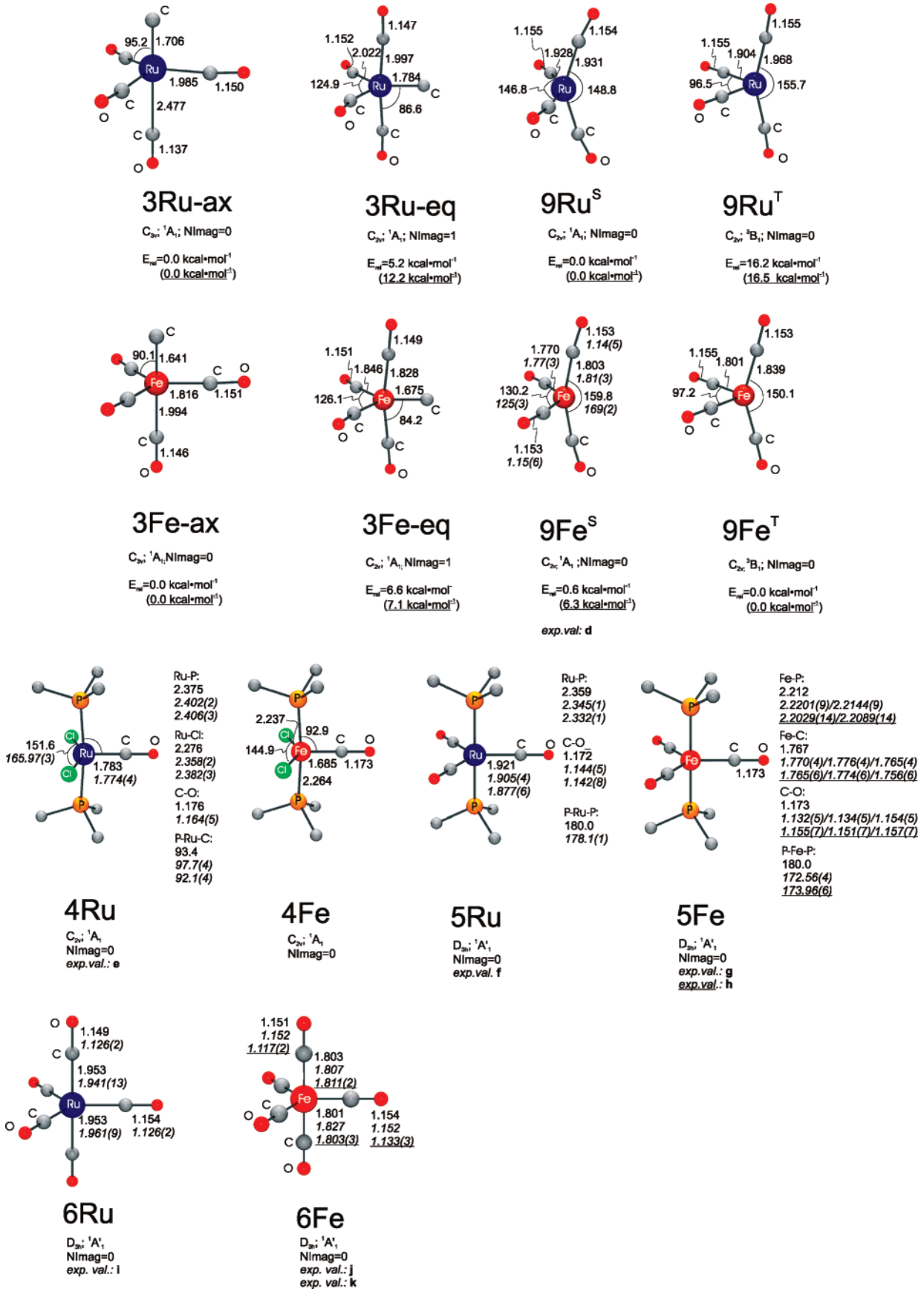

Figure 2. Optimized geometries (BP86/TZ2P) of the calculated compounds. Distances in Å, angles in deg. Experimental values are given in *italics*. The symmetry, the electronic state, and the number of imaginary modes (NImag) are given below each structure. In the case of isomeric structures and different spin states, relative energies (E_{rel}) are given at BP86/TZ2P and (CCSD(T)/BS1). a: (X-ray);[57] b: (X-ray);[16] c: (X-ray);[61] d: (electron diffraction);[66] e: (X-ray);[67] f: (X-ray);[68] g: (X-ray);[69] h: (X-ray);[70] i: (electron diffraction);[71] j: (electron diffraction);[72] k: (X-ray).[73] Hydrogen atoms of the PMe_3 ligands in compounds **4** and **5** are omitted for clarity reasons.

Table 1. Calculated Bond Dissociation Energies D_e[a] in kcal/mol; Zero-Point Vibrational Energy Corrected Values D_o Are Given in Parentheses

		D_e (D_o)	
molecule	no.	BP86/TZ2P	CCSD(T)/BS1
$Cl_2(PMe_3)Ru-C$	**1Ru**	146.5 (143.8)	-
$Cl_2(PMe_3)Fe-C$	**1Fe**	135.1 (132.3)	-
$Cl_2(PH_3)Ru-C$[b]	**1Ru(H)**	144.7 (142.8)	139.3
$Cl_2(PH_3)Fe-C$[b]	**1Fe(H)**	127.2 (124.0)	108.1
$(CO)_2(PMe_3)Ru-C$	**2Ru**	100.8 (99.6)	-
$(CO)_2(PMe_3)Fe-C$	**2Fe**	115.7 (113.6)	-
$(CO)_2(PH_3)Ru-C$[c]	**2Ru(H)**	96.6 (95.8)	92.7
$(CO)_2(PH_3)Fe-C$[c]	**2Fe(H)**	107.4 (104.7)	97.9
$(CO)_4Ru-C(ax)$	**3Ru-ax**	88.8 (88.9)	93.3
$(CO)_4Ru-C(eq)$	**3Ru-eq**	83.7 (82.9)	81.1
$(CO)_4Fe-C(ax)$	**3Fe-ax**	104.5 (102.7)	98.6
$(CO)_4Fe-C(eq)$	**3Fe-eq**	97.9 (95.7)	91.5
$Cl_2(PMe_3)Ru-CO$	**4Ru**	44.6 (41.2)	-
$Cl_2(PMe_3)Fe-CO$	**4Fe**	38.2 (34.7)	-
$Cl_2(PH_3)Ru-CO$[d]	**4Ru(H)**	45.2 (43.6)	36.3
$Cl_2(PH_3)Fe-CO$[d]	**4Fe(H)**	32.5 (30.0)	15.7
$(CO)_2(PMe_3)Ru-CO$	**5Ru**	40.3 (37.6)	-
$(CO)_2(PMe_3)Fe-CO$	**5Fe**	55.3 (51.6)	-
$(CO)_2(PH_3)Ru-CO$[e]	**5Ru(H)**	35.6 (33.8)	33.8
$(CO)_2(PH_3)Fe-CO$[e]	**5Fe(H)**	47.5 (44.1)	38.2
$(CO)_4Ru-CO$	**6Ru**	32.5 (30.4)	32.2
$(CO)_4Fe-CO$	**6Fe**	46.3 (43.1)	40.7

[a] Calculated with respect to the fragments in their electronic ground states (see text for discussion). [b]The TM−C bond lengths for the optimized structure at BP86/TZ2P are 1.663 Å for **1Ru(H)** and 1.549 Å for **1Fe(H)**. [c]The TM−C bond lengths for the optimized structure at BP86/TZ2P are 1.742 Å for **2Ru(H)** and 1.642 Å for **2Fe(H)**. [d]The TM−C bond lengths for the optimized structure at BP86/TZ2P are 1.776 Å for **4Ru(H)** and 1.696 Å for **4Fe(H)**. [e]The TM−C bond lengths for the optimized structure at BP86/TZ2P are 1.932 Å for **5Ru(H)** and 1.781 Å for **5Fe(H)**.

Eisenstein, Caulton and co-workers.[61] The authors reported about a joint experimental and theoretical study of the latter compound which is isolable but highly reactive. For example, it readily takes up CO yielding a tricarbonyl complex which is a homologue of the complex **5Ru** (see below). The surprisingly high stability of $[(CO)_2(P^tBu_2Me)_2Ru]$ and the nonplanar equilibrium geometry which is in good agreement with the calculated structure of $\mathbf{8Ru^S}$ (Figure 2) was explained with enhanced Ru → CO π-backdonation.[61] Figure 2 shows that the R−CO bond in the model complex $\mathbf{8Ru^S}$ and in the experimental compound $[(CO)_2(P^tBu_2Me)_2Ru]$ is indeed very short. The chemical reactivity of the latter complex toward various ligands L led the authors to conclude that $[(CO)_2(P^tBu_2Me)_2Ru]$ is not a very strong σ-Lewis acid as it might be anticipated because it is a 16VE complex, but that it relies heavily on the π-backbonding for the Ru−L binding. This hypothesis shall be examined (vide infra) in the section about bonding analysis.

Table 1 gives the calculated bond dissociation energies (BDE) at the BP86/TZ2P and CCSD(T)/BS1 levels of theory of the TM−C and TM−CO bonds of **1Ru**−**6Fe**. For some molecules we also carried out CCSD(T)/BS1 calculations. The fragments have been calculated at the respective electronic ground state. For the dissociation of the ligands these are ^3P for C and $^1\Sigma^+$ for CO. The metal fragments have either a singlet or a triplet ground state which are shown in Figure 2.

The DFT calculations predict that the metal−carbon bonds of **1Ru** and **1Fe** are very strong. The ruthenium complex has an even stronger bond (D_e = 146.5 kcal/mol) than the iron complex (D_e = 135.1 kcal/mol). This is remarkable because iron complexes usually have stronger metal−ligand bonds than ruthenium complexes. For example, experimental and theoretical work has shown that the BDE of one CO ligand of $[Fe(CO)_5]$ is significantly higher than that of $[Ru(CO)_5]$.[58−60] The dissociation of the carbon ligand of **1Ru** gives the metal fragment $\mathbf{7Ru^S}$ in the electronic singlet state which has a tetrahedral arrangment of the four ligands at the metal. The rupture of the Fe−C bond of **1Fe** yields the metal fragment $\mathbf{7Fe^T}$ in the electronic triplet state which has a planar geometry at the metal. The DFT results for the BDE of **1Ru** and **1Fe** are probably slightly too large. We calculated the BDE of the model compounds **1Ru(H)** and **1Fe(H)** where the phosphane ligands are modeled by PH_3 because our computational resources made it not possible for us to carry out CCSD(T)/BS1 calculations of **1Ru** and **1Fe**. Table 1 shows that the bond energies of **1Ru(H)** and **1Fe(H)** which are calculated at BP86/TZ2P are a bit smaller than those for **1Ru** and **1Fe**. The CCSD(T)/BS1 calculations give lower values for the BDE of **1Ru(H)** and **1Fe(H)** particularly for the iron compound. The theoretical data suggest that the bond energy of the metal−carbon bond in **1Ru** is approximately D_e ∼140 kcal/mol and D_e ∼115 kcal/mol in **1Fe**.

The metal−carbon bonds in the 18VE complexes **2Ru** and **2Fe** are weaker than those in the 16VE species **1Ru** and **1Fe**. Another difference between the two pairs is that the Fe−C bond in the iron complex **2Fe** at BP86/TZ2P is stronger (D_e = 115.7 kcal/mol) than the Ru−C bond in **2Ru** (D_e = 100.75 kcal/mol), while the opposite order is calculated for **1Ru** and **1Fe** (Table 1). The same trend is calculated at BP86/TZ2P and CCSD(T)/BS1 for the molecules with the PH_3 ligands **2Ru(H)** and **2Fe(H)** which have slightly weaker TM−C bonds than those for **1Ru** and **1Fe**. The calculated values shown in Table 1 suggest that the bond energy of the metal−carbon bond in the 18VE carbon complexes is approximately D_e ∼95 kcal/mol for **2Ru** and D_e ∼105 kcal/mol for **2Fe**.

The tetracarbonyl carbon complexes $[(CO)_4Ru(C)]$ (**3Ru**) and $[(CO)_4Fe(C)]$ (**3Fe**) have weaker TM−C bonds than **2Ru** and **2Fe**. Table 1 shows that the BDE of the carbon ligand in the equatorial position of **3Ru-eq** and **3Fe-eq** is ∼17 kcal/mol less than that in **2Ru** and **2Fe**. The equatorial isomers **3TM-eq** are transition states, but the values for the BDE of the axial energy minima **3Ru-ax** and **3Fe-ax** are still smaller than those for the phosphane complexes **2Ru** and **2Fe**.

The calculated bond energies for the carbonyl complexes **4Ru**−**6Fe** shown in Table 1 indicate that the equatorial CO ligand is more weakly bonded than the carbon ligand in the respective complexes **1Ru**−**3Fe**. The theoretically predicted bond dissociation energies of the ligand C in the latter compounds are more than twice as high as the BDE of CO in the former molecules. The calculated values for the BDE of the pentacarbonyl complexes are in good agreement with the experimental bond dissociation energies for $[Ru(CO)_5]$ (27.6 ± 0.4 kcal/mol)[58] and $[Fe(CO)_5]$ (41 ± 2 kcal/mol).[59]

An important result comes to the fore when the theoretical BDE values for the 16VE complexes **1Ru**, **1Fe**, **4Ru**, **4Fe** are compared with the data for the 18VE complexes **2Ru**, **2Fe**, **3Ru**, **3Fe**, **5Ru**, **5Fe**, **6Ru**, **6Fe**. The calculations predict that the 16VE

(57) Hejl, A.; Trnka, T. M.; Day, M. W.; Grubbs, R. H. *Chem. Commun.* **2002**, 2524.
(58) Huq, R.; Poe, A. J.; Chawla, S. *Inorg. Chim. Acta* **1980**, *38*, 121.
(59) Lewis, K. E.; Golden, D. M.; Smith, G. P. *J. Am. Chem. Soc.* **1984**, *106*, 3905.
(60) Ehlers, A.; Frenking, G. *Organometallics* **1995**, *14*, 423.

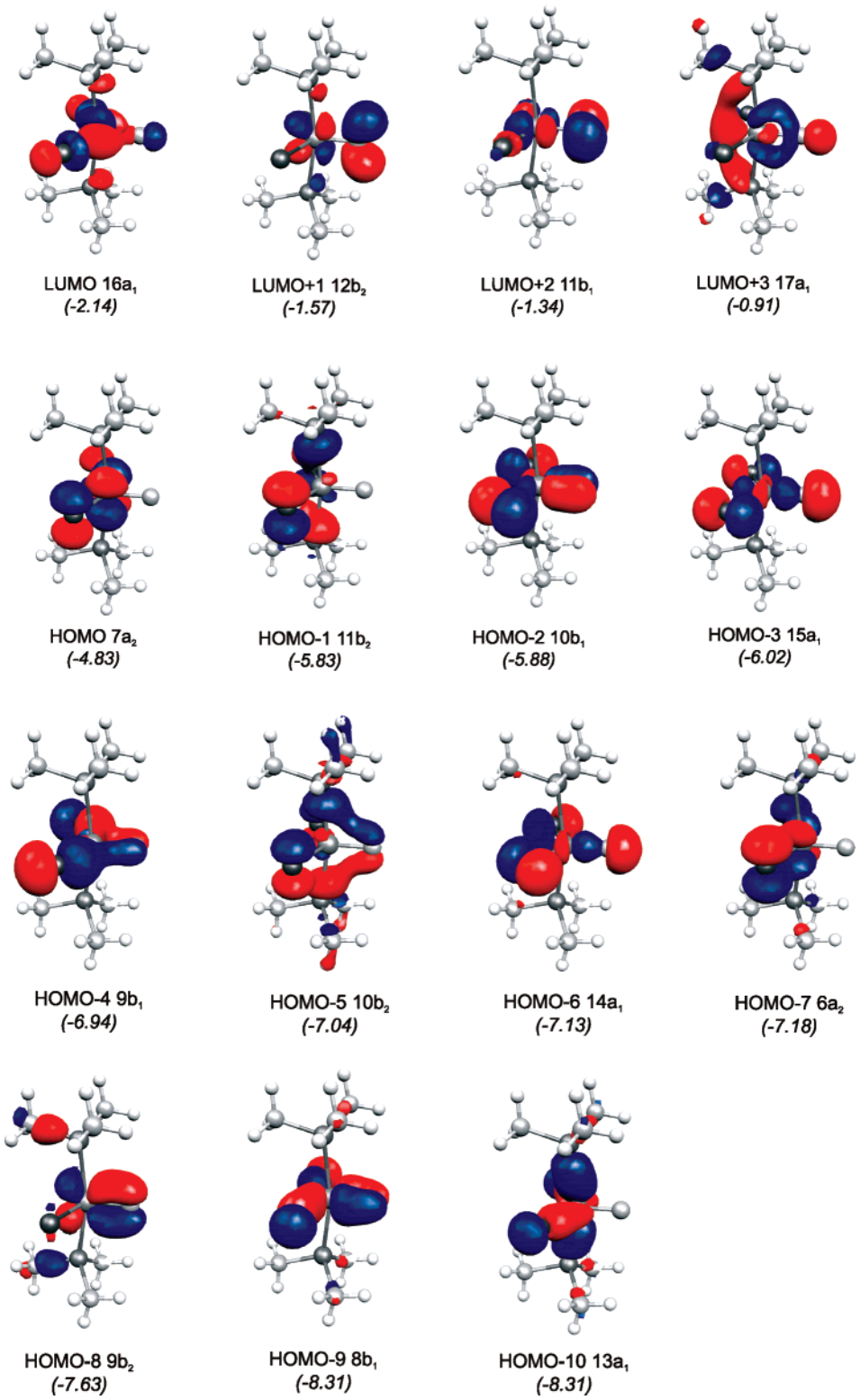

Figure 3. Plot of the 11 highest lying occupied molecular orbitals and four lowest lying vacant MOs of $[(PMe_3)_2Cl_2Ru(C)]$ (**1Ru**). The calculated eigenvalues (BP86/TZ2P) of the orbitals are given in parentheses (in eV).

ruthenium complexes always have a higher BDE than the iron complexes, while the 18VE ruthenium complexes always have a lower BDE than the iron homologues.

Analysis of the Bonding Situation

It is instructive for the numerical analysis of the metal−C bonding analysis to present and to shortly discuss the molecular orbitals of the model compound $[Cl_2(PMe_3)_2Ru(C)]$ (**1Ru**). Figure 3 displays the 11 highest lying MOs of **1Ru** which include all orbitals that are relevant for the Ru−C bonding.

The shape of the valence orbitals indicates that there are seven occupied MOs which contribute to the [Ru]−carbon bond, two σ orbitals and five π orbitals. The HOMO−3 ($15a_1$) and HOMO−6 ($14a_1$) orbitals come from the bonding and anti-

Table 2. Calculated Charge Distribution Given by the Natural Population Analysis at BP86/def2-TZVPP//BP86/TZ2P[a]

molecule	no.	P(TM–C)	q(TM)	q(C)	$2s(C)_\sigma$	$2p_z(C)_\sigma$	$2p_x(C)_{\pi\|\|}$	$2p_y(C)_{\pi\perp}$	q(CO)	$\Delta q(CO)_\sigma$	$\Delta q(CO)_{\pi\|\|}$	$\Delta q(CO)_{\pi\perp}$
$Cl_2(PMe_3)Ru-C$	**1Ru**	2.1	−0.08	0.04	1.81	0.93	0.66	0.54	-	-	-	-
$Cl_2(PMe_3)Fe-C$	**1Fe**	2.0	−0.19	0.12	1.82	0.92	0.59	0.53	-	-	-	-
$(CO)_2(PMe_3)Ru-C$	**2Ru**	1.6	−0.38	−0.23	1.80	1.23	0.77	0.40	-	-	-	-
$(CO)_2(PMe_3)Fe-C$	**2Fe**	1.4	−0.63	−0.19	1.78	1.27	0.70	0.42	-	-	-	-
$(CO)_4Ru-C(ax)$	**3Ru-ax**	1.8	−0.20	0.04	1.80	1.04	0.55	0.55	-	-	-	-
$(CO)_4Ru-C(eq)$	**3Fe-ax**	1.4	−0.53	0.10	1.80	1.13	0.47	0.47	-	-	-	-
$(CO)_4Fe-C(ax)$	**3Ru-eq**	1.5	−0.30	−0.02	1.83	1.20	0.70	0.27	-	-	-	-
$(CO)_4Fe-C(eq)$	**3Fe-eq**	1.2	−0.59	0.08	1.82	1.19	0.62	0.28	-	-	-	-
$Cl_2(PMe_3)Ru-CO$	**4Ru**	1.4	−0.12	-	-	-	-	-	0.09	+0.71	−0.33	−0.28
$Cl_2(PMe_3)Fe-CO$	**4Fe**	1.2	−0.07	-	-	-	-	-	0.08	+0.64	−0.27	−0.27
$(CO)_2(PMe_3)Ru-CO$	**5Ru**	0.8	−0.47	-	-	-	-	-	−0.14	+0.42	−0.35	−0.18
$(CO)_2(PMe_3)Fe-CO$	**5Fe**	0.7	−0.65	-	-	-	-	-	−0.10	+0.45	−0.32	−0.21
$(CO)_4Ru-CO_{eq}$	**6Ru**	0.7	−0.32	-	-	-	-	-	0.02	+0.42	−0.28	−0.11
$(CO)_4Fe-CO_{eq}$	**6Fe**	0.6	−0.58	-	-	-	-	-	0.08	+0.47	−0.25	−0.13

[a] P(TM−C) denotes the Wiberg bond order on the basis of the Natural Atomic Orbitals (NAOs) between atoms TM and C. q(E) Gives the partial charge in au for the metal atom TM, the terminal C atom, or the CO fragment. 2s(C)-$2p_z$(C) are the occupation numbers of the NAOs for the terminal C atom. Δq(CO)gives the difference in the occupation numbers of the NAOs of the bound CO (2*s*, $2p_x$, $2p_y$, and $2p_z$ of C and O) and the values for the free CO molecule. Positive values for Δq(CO) stand for higher occupation numbers in free CO.

bonding combination of the d_{z^2} ruthenium orbital with the chlorine p(σ) lone-pair orbitals. Both MOs contribute to the Ru−C σ bond. Two orbitals describe the Ru−C π interactions in the Cl−Ru−Cl plane ($\pi_{||}$). The HOMO−2 ($10b_1$) and HOMO−9 ($8b_1$) orbitals which come from different Cl−Ru−Cl b_1 fragment orbitals all possess bonding contribution to the Ru−C $\pi_{||}$ bond. The HOMO−8 ($9b_2$) orbital is a Ru−C π orbital in the P−Ru−P plane ($\pi_\perp$). The remaining π orbitals HOMO−4 ($9b_1$) and HOMO−5 ($10b_2$) have only small contributions at the carbon ligand atom. Closer inspection of the shape (Figure 3) and coefficients shows that the latter orbital mainly comes from a bonding combination of ligand orbitals (Cl in HOMO-4 and PMe_3 in HOMO-5) with the carbon atom. They have negligible coefficients at the metal atom. Figure 3 also shows the four lowest lying vacant orbitals of **1Ru**. Note that the LUMO ($16a_1$) is antibonding with respect to the Ru−C bond. This is important for understanding the changes in the bonding situation of the 18 VE complexes which are discussed below where this orbital is occupied and becomes the HOMO. The π orbitals LUMO+1 ($12b_2$) and LUMO+2 ($11b_1$) and the occupied σ orbital HOMO−3 ($15a_1$) are perfectly suited to serve as ligand orbitals for binding of **1Ru** to another transition metal fragment. Indeed, the complex [**1Ru**−$Mo(CO)_5$] where **1Ru** binds with $Mo(CO)_5$ through the carbon atom has been isolated.[17] The pictorial representation of the orbital shall now be complemented with a numerical analysis of the electronic structure of the complexes.

We first discuss the NBO results shown in Table 2 which give information about the charge distribution in the molecules. The results of the charge partitioning shall then be complemented with the data for the energy partitioning given by the EDA.

The NBO results for the carbon complexes indicate that the ruthenium and iron species **1Ru** and **1Fe** have the largest values for the metal−carbon bond orders P(TM−C) shown in Table 2. The 18VE complexes have smaller P(TM−C) values than the 16VE compounds. The Ru−C bonds have always larger bond orders than the respective Fe−C bonds which agrees with the calculated bond dissociation energies of **1Ru** and **1Fe** but not with the BDE values of the other carbon complexes (Table 1). It will be shown below that the P(TM−C) values correlate much better with the intrinsic interaction energies ΔE_{int} between the frozen fragments. This is reasonable because the BDE may be strongly influenced by the relaxation energy of the fragments. From the bond order values one may conclude that **3Ru-ax** is the most promising candidate from the investigated compounds which may become isolated, because the large value for P(Ru−C) = 1.8 suggests a very strong ruthenium−carbon bond. This is misleading. It was shown above that the Ru−CO bond which is *trans* to Ru−C is very long and the CO ligand may dissociate and [$(CO)_3$RuC] would be formed which might become isolated.

The atomic partial charges indicate that the metal atom always carries a small negative charge and that Fe is more negatively charged than Ru except for **4Ru** and **4Fe**. Further breakdown of the atomic charges into orbital charges shows that the p(π) orbitals of the carbon ligand are significantly occupied. If the ligand carbon atom is interpreted as a closed-shell donor−acceptor species with the electron configuration $(2s)^2(2p_{z(\sigma)})^2(2p_{x(\pi)})^0(2p_{y(\pi)})^0$, then it behaves as a very strong σ donor and also as a strong π acceptor. There are interesting changes in the carbon σ and π charges of the 16VE complexes **1Ru** and **1Fe** and the 18 VE complexes **2Ru** and **2Fe** which give a first hint of the difference between the metal−carbon bonding in the two classes of compounds. The occupation of the $2p_{z(\sigma)}$(C) orbital in the 16VE complexes **1Ru** and **1Fe** (0.93; 0.92) is significantly smaller than that in the 18VE species **2Ru** and **2Fe** (1.23; 1.27), while the total $2p_\pi$(C) occupation in the former species (1.20; 1.12) is only slightly larger than or equal to that in the latter (1.17; 1.12). This indicates that the σ donation in the 16VE compounds is clearly stronger than that in the 18 VE species, while the π backdonations in the two classes are not very different. This conclusion is supported by the EDA results which are given below.

A comparison with the carbonyl complexes shows that the CO ligand is a much weaker σ donor and π acceptor than carbon. It remains to be seen if the donor−acceptor description which is valid for carbonyl complexes[21,23,62] may be applied for the carbon complexes as well. In order to address this question and to analyze the energy contributions which come not only from orbital interactions but also from electrostatic bonding, we will in the following present and discuss the EDA results.

(61) Ogasawara, M.; Macgregor, S. A.; Streib, W. E.; Folting, K.; Eisenstein, O.; Caulton, K. G. *J. Am. Chem. Soc.* **1996**, *118*, 10189.
(62) Diefenbach, A.; Bickelhaupt, F. M.; Frenking, G. *J. Am. Chem. Soc.* **2000**, *122*, 6449.

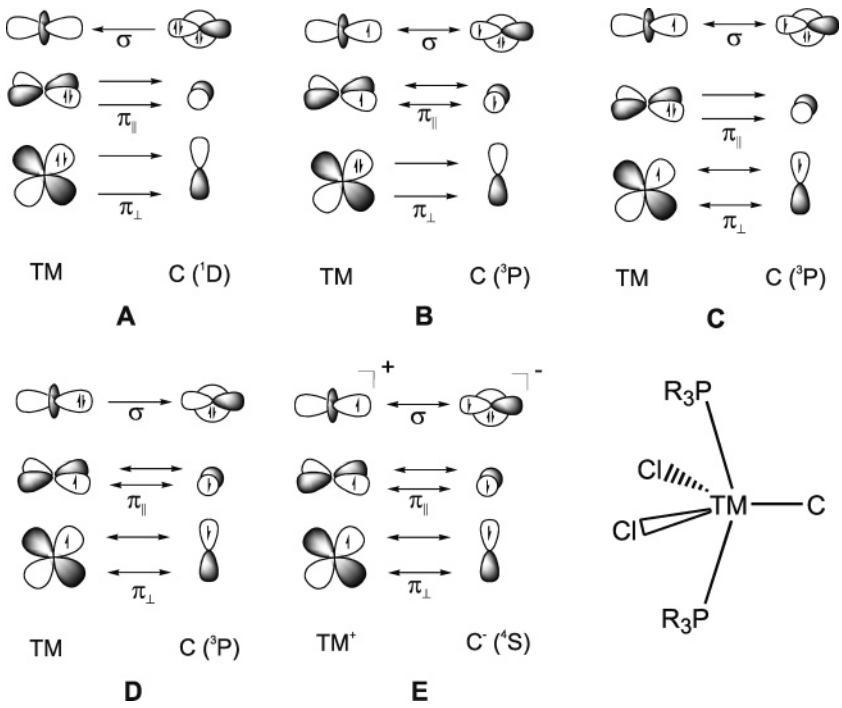

Figure 4. Schematic representation of the electron configurations of the interacting fragments A−E which are used in the EDA calculations.

Table 3. Energy Decomposition Analysis at BP86/TZ2P of the Ruthenium−Carbon Bond in the Complex **1Ru** Using Different Fragment Pairs A−E as Shown in Figure 4 (All Energies in kcal mol^{-1})

fragment	A	B	C	D	E
ΔE_{int}	−245.0	−170.4	−197.9	−183.4	−306.9
ΔE_{Pauli}	499.1	429.1	437.4	366.0	526.5
ΔE_{Elstat}[a]	−410.0 (55.1%)	−289.9 (48.4%)	−301.4 (47.4%)	−183.1 (33.3%)	−493.9 (59.3%)
ΔE_{Orb}[a]	−334.1 (44.9%)	−309.6 (51.6%)	−333.9 (52.6%)	−366.3 (66.7%)	−339.6 (40.7%)
$\Delta a_1(\sigma)$[b]	−140.1 (41.9%)	−142.0 (45.9%)	−144.9 (43.4%)	−210.5 (57.5%)	−146.6 (43.2%)
$\Delta a_2(\delta)$[b]	−0.2 (0.1%)	−0.3 (0.1%)	−0.3 (0.1%)	−0.4 (0.1%)	−1.7 (0.5%)
$\Delta b_1(\pi_{\|\|})$[b]	−105.1 (31.5%)	−75.4 (24.4%)	−108.6 (32.5%)	−75.2 (20.5%)	−90.5 (26.7%)
$\Delta b_2(\pi_\perp)$[b]	−88.8 (26.6%)	−91.9 (29.7%)	−80.2 (24.0%)	−80.3 (21.9%)	−100.8 (29.7%)
ΔE_{Prep}	98.5	23.9	51.4	36.9	160.4
$-D_e$	−146.5	−146.5	−146.5	−146.5	−146.5

[a] The value in parentheses gives the percentage contribution to the total attractive interactions ($\Delta E_{Elstat} + \Delta E_{Orb}$). [b]The value in parentheses gives the percentage contribution to the total orbital interactions.

We first consider the ruthenium−carbon bonding situation in **1Ru** which was analyzed with the EDA using five different pairs of fragments A−E which are shown in Figure 4. The pertinent EDA results are given in Table 3.

The fragment pair A describes donor−acceptor interactions between the carbon ligand atom with the electron configuration $(2s)^2(2p_{z(\sigma)})^2(2p_{x(\pi)})^0(2p_{y(\pi)})^0$ and the metal fragment [$(PMe_3)_2Cl_2Ru$] where both d(π) orbitals of Ru are doubly occupied. The Ru−C interactions in model A comply with the Dewar−Chatt−Duncanson (DCD) model which considers Ru ← C σ donation and Ru → C π backdonation as crucial bonding components.[63−65] The bonding situation is similar to the description given for Fischer carbynes (Figure 1b), but the fragments for the metal−C bond in model A are neutral. The orientation of the molecule with respect to the molecular planes is also shown in Figure 4. The π bonding in the Cl−Ru−Cl plane is denoted as $\pi_{||}$, while π bonding in the P−Ru−P plane is denoted as $\pi_\perp$. In the bonding model B the carbon ligand atom has the electron configuration $(2s)^2(2p_{z(\sigma)})^1(2p_{x(\pi)})^1(2p_{y(\pi)})^0$ and the metal fragment has the configuration $d_z2(\sigma)^1d_{xz}(\pi)^1d_{yz}(\pi)^2$. A similar bonding situation is described in model C where only the occupation of the π orbitals is reversed. Both models describe a bonding situation with two electron-sharing bonds, one of them possessing σ symmetry and the other π symmetry, and one Ru → C π donor−acceptor bond. The latter orbital is in B in the P−Ru−P plane ($\pi_\perp$), while in C it is in the Cl−Ru−Cl plane ($\pi_{||}$). Bonding model D possesses one Ru → C σ donor bond and two Ru−C electron-sharing π bonds between the carbon ligand which has the electron configuration $(2s)^2(2p_{z(\sigma)})^0(2p_{x(\pi)})^1(2p_{y(\pi)})^1$ and the metal fragment where Ru has the configuration $d_z2(\sigma)^2d_{xz}(\pi)^1d_{yz}(\pi)^1$. Finally, bonding model E describes three electron-sharing bonds, one of them having σ and the other π symmetry. The latter situation is similar to the bonding situation for Schrock carbynes shown in Figure 1d, but the fragments for the TM−C bond in model E are charged.

The EDA data given in Table 3 suggest that the best bonding model for the ruthenium−carbon interactions in **1Ru** is model

(63) Dewar, M. J. S. *Bull. Soc. Chim. Fr.* **1951**, *18*, C79.
(64) Chatt, J.; Duncanson, L. A. *J. Chem. Soc.* **1953**, 2929.
(65) Frenking, G. In *Modern Coordination Chemistry: The Legacy of Joseph Chatt*; Leigh, G. J., Winterton, N., Eds.; The Royal Society: London, 2002; p 111.

Table 4. Energy Decomposition Analysis at BP86/TZ2P of the Ru−C Bond in the Complexes **1Ru**, **2Ru**, and **3Ru-eq** Using Different Fragment Pairs A and B as Shown in Figure 4 (Energies in kcal mol^{-1})

	A			B		
	1Ru	**2Ru**	**3Ru-eq**	**1Ru**	**2Ru**	**3Ru-eq**
ΔE_{int}	−245.0	−184.1	−159.2	−170.4	−137.1	−114.8
ΔE_{Pauli}	499.1	461.1	421.9	429.1	441.7	377.2
ΔE_{Elstat}[a]	−410.0 (55.1%)	−378.5 (58.7%)	−342.2 (58.9%)	−289.9 (48.4%)	−291.1 (50.3%)	−247.5 (50.3%)
ΔE_{Orb}[a]	−334.1 (44.9%)	−266.7 (41.3%)	−238.9 (41.1%)	−309.6 (51.6%)	−287.7 (49.7%)	−244.4 (49.7%)
$\Delta a_1(\sigma)$[b]	−140.1 (41.9%)	−95.5 (35.8%)	−101.1 (42.3%)	−142.0 (45.9%)	−155.3 (54.0%)	−134.7 (55.1%)
$\Delta a_2(\delta)$[b]	−0.2 (0.1%)	−0.1 (0.0%)	−0.1 (0.0%)	−0.3 (0.1%)	−0.2 (0.1%)	−0.2 (0.1%)
$\Delta b_1(\pi_{\|})$[b]	−105.1 (31.5%)	−105.4 (39.5%)	−91.9 (38.5%)	−75.4 (24.4%)	−64.4 (22.4%)	−63.1 (25.8%)
$\Delta b_2(\pi_{\perp})$[b]	−88.8 (26.6%)	−65.7 (24.6%)	−45.8 (19.2%)	−91.9 (29.7%)	−67.8 (23.6%)	−46.4 (19.0%)
ΔE_{Prep}	98.5	83.3	75.5	23.9	36.3	31.1
$-D_e$	−146.5	−100.8	−83.7	−146.5	−100.8	−83.7

[a] The value in parentheses gives the percentage contribution to the total attractive interactions ($\Delta E_{Elstat} + \Delta E_{Orb}$). [b]The value in parentheses gives the percentage contribution to the total orbital interactions.

B. This becomes evident from the calculated values for the orbital interaction. The ΔE_{orb} value in model B (−309.6 kcal/mol) is the smallest among the five different models. It means that the electron configuration of the fragments which is shown for B in Figure 4 experiences the smallest change upon the Ru−C bond formation. Since model B also requires the least amount of electronic excitation and geometry changes of all models given by the ΔE_{prep} values (Table 3), it is clearly the most appropriate choice of interacting fragments. Model B indicates that the $\pi_{\|}$ bond between ruthenium and carbon which is in the Cl−Ru−Cl plane is an electron-sharing bond, while the $\pi_{\perp}$ bond in the P−Ru−P plane is a donor−acceptor bond. The EDA shows that the latter interaction is stronger ($\Delta b_2(\pi_{\perp}) = -91.9$ kcal/mol) than the former ($\Delta b_1(\pi_{\|}) = -75.4$ kcal/mol). If both π components come from donor−acceptor interactions as in the case of model A, the $\pi_{\|}$ bond in the Cl−Ru−Cl plane is stronger ($\Delta b_1(\pi_{\|}) = -105.1$ kcal/mol) than that in the P−Ru−P plane ($\Delta b_2(\pi_{\perp}) = -88.8$ kcal/mol). It is interesting to note that the strength of the σ interactions in models A ($\Delta a_1(\sigma) = -140.1$ kcal/mol) and B ($\Delta a_1(\sigma) = -142.0$ kcal/mol) are not very different from each other. The same holds true for all orbital components of models A and C which leads to nearly identical ΔE_{orb} values for the interacting fragments. The EDA results using models D and E give clearly larger values for ΔE_{orb} than those using model B and shall therefore not be discussed in detail. It is noteworthy, however, that the ΔE_{orb} value using the Schrock carbyne-type model E (−339.6 kcal/mol) is similar to the value using model A (−334.1 kcal/mol) which describes a Fischer carbyne-type bonding situation as shown in Figure 1b. The EDA data suggest that both models are less appropriate for describing the Ru−C bond in **1Ru** than model B.

The EDA results for **1Ru** shall be compared with the data for the other ruthenium−carbon complexes in order to elucidate the electronic factors which contribute to the stability of the compounds. Table 4 gives the EDA results for the 16VE complex **1Ru** and the 18VE complexes **2Ru** and **3Ru-eq** using the fragment pairs A and B. Inspection of the EDA results for the latter molecules showed that the bonding model A gives smaller ΔE_{orb} values for the 18VE species than model B, while models C−E give even larger numbers for the orbital interaction. Therefore we present and discuss only EDA results which come from using models A and B. Although the axial isomer **3Ru-ax** is lower in energy than the equatorial form, we calculated **3Ru-eq** in order to compare it with the bonding situation in **1Ru** and **2Ru** which have the carbon ligand in the equatorial position.

Pivotal differences between the bonding situation in the 16VE and 18VE complexes are revealed when the EDA results of **1Ru** and **2Ru** using the same bonding model A are compared with each other. Although the Ru−C binding interactions in **1Ru** are better described by model B, it is reasonable to use for the comparison the same bonding model for both compounds. Table 4 shows that the Ru−C bond in **2Ru** is significantly weaker than that in **1Ru**. The total interaction energy in the 18VE complex is $\Delta E_{int} = -184.1$ kcal/mol, which is 60.9 kcal/mol less than that in the 16VE species ($\Delta E_{int} = -245.0$ kcal/mol). The theoretically predicted BDE of the latter is also much higher ($D_e = 146.5$ kcal/mol) than that in the former compound ($D_e = 100.8$ kcal/mol).

Table 4 shows that the relative contributions of the attractive terms ΔE_{elstat} and ΔE_{orb} in **1Ru** and **2Ru** are not very different from each other. In particular the values for the $\pi_{\|}$ bonding in **1Ru** ($\Delta b_1(\pi_{\|}) = -105.1$ kcal/mol) and **2Ru** ($\Delta b_1(\pi_{\|}) = -105.4$ kcal/mol) are nearly the same. This is somewhat surprising, because the $\pi_{\|}$ plane in **1Ru** is the Cl−Ru−Cl plane, while in **2Ru** it is the CO−Ru−CO plane. This means that the donor−acceptor interactions in the $\pi_{\|}$ plane change very little when chlorine becomes substituted by CO. A larger change is calculated for the interactions in the $\pi_{\perp}$ plane (P−Ru−P) where the π backdonation in **2Ru** is clearly smaller ($\Delta b_2(\pi_{\perp}) = -65.7$ kcal/mol) than that in **1Ru** ($\Delta b_2(\pi_{\perp}) = -88.8$ kcal/mol). However, the largest change in the orbital contribution between **1Ru** and **2Ru** is calculated for the σ interaction and not for the π interaction! Table 4 shows that the $\Delta a_1(\sigma)$ contribution in **2Ru** is much smaller (−95.5 kcal/mol) than that in **1Ru** (−140.1 kcal/mol). This is in agreement with the previously discussed results of the charge decomposition analysis which showed that σ donation in **1Ru** is much bigger than in **2Ru**, while the difference between the π charges are quite small. The much weaker Ru−C σ bonding in the 18VE complex using model A[74] can be explained with the occupation of the σ antibonding

(66) Ihee, H.; Cao, J.; Zewail, A. H. *Angew. Chem, Int. Ed.* **2001**, *40*, 1532; *Angew. Chem.* **2001**, *113*, 1580.
(67) Huang, D.; Streib, W. E.; Bollinger, J. C.; Caulton, K. G.; Winter, R. F.; Scheiring, T. *J. Am. Chem. Soc.* **1999**, *121*, 8087.
(68) Jones, R. A.; Wilkinson, G.; Galas, A. M. R.; Hursthouse, M. B.; Malik, K. M. A. *J. Chem. Soc., Dalton Trans.* **1980**, 1771.
(69) Glaser, R.; Yoo, Y. H.; Chen, G. S.; Barnes, C. L. *Organometallics* **1994**, *13*, 2578.
(70) Glaser, R.; Haney, P. E.; Barnes, C. L. *Inorg. Chem.* **1996**, *35*, 1758.
(71) Huang, J.; Hedberg, K.; Davis, H. B.; Pomeroy, R. K. *Inorg. Chem.* **1990**, *29*, 3923.
(72) Beagley, B.; Schmidling, D. G. *J. Mol. Struct.* **1974**, *22*, 466.
(73) Braga, D.; Grepioni, F.; Orpen, A. G. *Organometallics* **1993**, *12*, 1481.

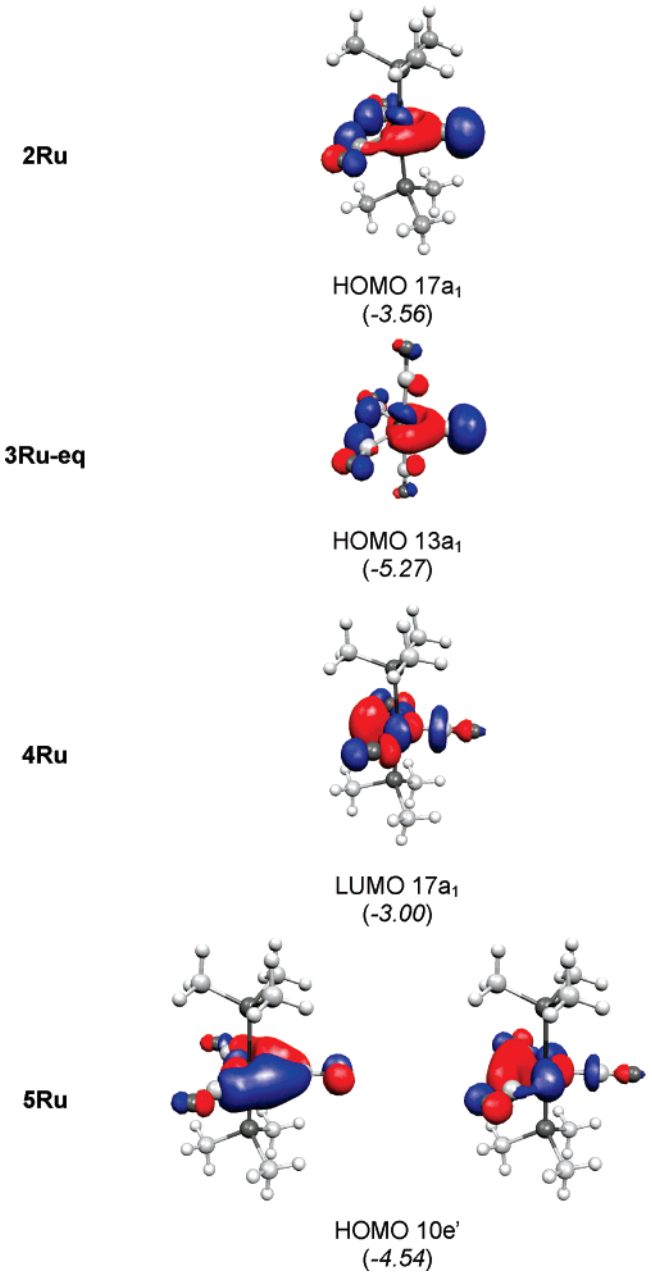

Figure 5. Plot of the highest lying occupied molecular orbitals of $[(PMe_3)_2(CO)_2Ru(C)]$ (**2Ru**), $[(CO)_4Ru(C)]$ (**3Ru-eq**), $[(PMe_3)_2Ru(CO)_3]$ (**5Ru**), and the lowest lying vacant MO of $[(PMe_3)_2Cl_2Ru(CO)]$ (**4Ru**). The calculated eigenvalues (BP86/TZ2P) of the orbitals are given in parentheses (in eV).

LUMO ($16a_1$) in the 16VE complex **1Ru** (see Figure 3) which becomes the HOMO in **2Ru** (Figure 5). The difference between the $\Delta a_1(\sigma)$ values of the two complexes is 44.6 kcal/mol which nearly matches the difference between the bond dissociation energies (45.7 kcal/mol). The agreement is, however, fortuitous. The difference between the latter value comes also from the change in the preparation energies of the fragments ΔE_{prep} which amount to 15.2 kcal/mol (Table 4). Nevertheless, the EDA data suggest that the weakening of the Ru−C bonding interactions in the 18VE complex **2Ru** comes mainly from the occupation of the σ antibonding HOMO (Figure 5) which is vacant in **1Ru**.[74] Figure 5 shows also the HOMO of **3Ru-eq** which has a similar shape in the Ru−C bonding region as the HOMO of **2Ru** and the LUMO of **1Ru**. The congruent orbitals of the iron complexes **1Fe**, **2Fe**, and **3Fe-eq** resemble those of the ruthenium complexes, and therefore, they are not shown.

Figure 6 shows an orbital correlation diagram for the donor−acceptor interactions between a carbon atom with the electron configuration $(2s)^2(2p_{z(\sigma)})^2(2p_{x(\pi)})^0(2p_{y(\pi)})^0$ and the metal fragments $[(PMe_3)_2(CO)_2Ru]$ (left) and $[(PMe_3)_2Cl_2Ru]$ (right) with the appropriate electron configurations. The relative ordering of the orbital energy levels have directly been taken from the calculated orbitals which are shown in Figure 3. From the orbital interaction diagram it becomes immediately obvious why the $a_1(\sigma)$ interactions are more important than the $b_1(\pi_{||})$ and $b_2(\pi_{\perp})$ interactions. The d^8 metal fragment $[(PMe_3)_2(CO)_2Ru]$ has the electron configuration $(a_1)^2(a_2)^2(b_1)^2(b_2)^2$ while the d^6 metal fragment $[(PMe_3)_2Cl_2Ru]$ has the electron configuration $(a_1)^0(a_2)^2(b_1)^2(b_2)^2$. The latter fragment is a much better σ acceptor than the former because it has an empty low lying $14a_1$ orbital which is a metal d_{z^2} AO. This yields strong $(PMe_3)_2Cl_2Ru\leftarrow C$ σ donation in **1Ru**. The pivotal difference between **1Ru** and **2Ru** is that in the metal fragment of the latter complex the $15a_1$ orbital is occupied. Figure 6 shows that the occupied $17a_1$ in **2Ru** is rather high in energy. As mentioned above, the EDA results in Table 4 suggest that the occupation of the latter orbital weakens the overall $a_1(\sigma)$ interactions. The stronger $b_2(\pi_{\perp})$ donor−acceptor interactions in **1Ru** can be explained with the polarization of the $11b_2$ donor orbital (Figure 6). The phosphane ligands in the 16VE complex are bent toward the chlorine ligands which enlarges the lobes in the metal fragment toward the empty coordination site, while the phosphane ligands in the 18 VE complex are bent away from the CO ligands. Thus, charge and energy decomposition analysis suggest that the stronger and shorter Ru−C bond in the 16VE complex **1Ru** than that in the 18VE complex **2Ru** comes from the stronger Ru−C σ bonding which may be the reason that the former compound could become isolated.

The EDA data for **2Ru** and **3Ru-eq** using model A show that the substitution of PMe_3 by CO weakens the Ru−C interactions in the latter molecule by ∼15 kcal/mol. The bond weakening can be traced back to less $Ru\rightarrow C$ π backdonation in **3Ru-eq** where both components $\Delta b_2(\pi_{\perp})$ and $\Delta b_1(\pi_{||})$ have significantly smaller values than those in **2Ru**. The former compound has stronger $Ru \leftarrow C$ σ donation ($\Delta a_1(\sigma) = -101.1$ kcal/mol) than the latter ($\Delta a_1(\sigma) = -95.5$ kcal/mol), but this does not compensate for the loss in π bonding.

The EDA data in Table 5 show that the Fe−C bond in the 16VE complex **1Fe** when compared to Ru−C in **1Ru** is weaker and has a lower BDE value. This result comes from comparing the EDA results using models A and B alike. In contrast to this, the BDEs of the 18VE iron complexes which shall be discussed using the appropriate model A results are larger in **2Fe** ($D_e = 115.7$ kcal/mol) and **3Fe-eq** ($D_e = 97.9$ kcal/mol) than in the ruthenium complexes **2Ru** ($D_e = 100.8$ kcal/mol) and **3Ru-eq** ($D_e = 83.7$ kcal/mol), while the ΔE_{int} values of the iron complexes are only slightly smaller than those of the ruthenium species. Inspection of the energy contributions to the

(74) The bonding model B does not give a decrease of the σ orbital term when one goes from **1Ru** to **2Ru** because the attractive $\Delta a_1(\sigma)$ contribution comes from electron-sharing interactions which are not directly influenced by the occupation of the $17a_1$ orbital. There is even a slight increase in **2Ru** ($\Delta a_1(\sigma) = -155.3$ kcal/mol) compared with **1Ru** ($\Delta a_1(\sigma) = -142.0$ kcal/mol) which comes from better energy matching and rehybridization. This clearly shows that bonding model A is better suited for a comparison of the 16VE complexes with the 18VE complexes.

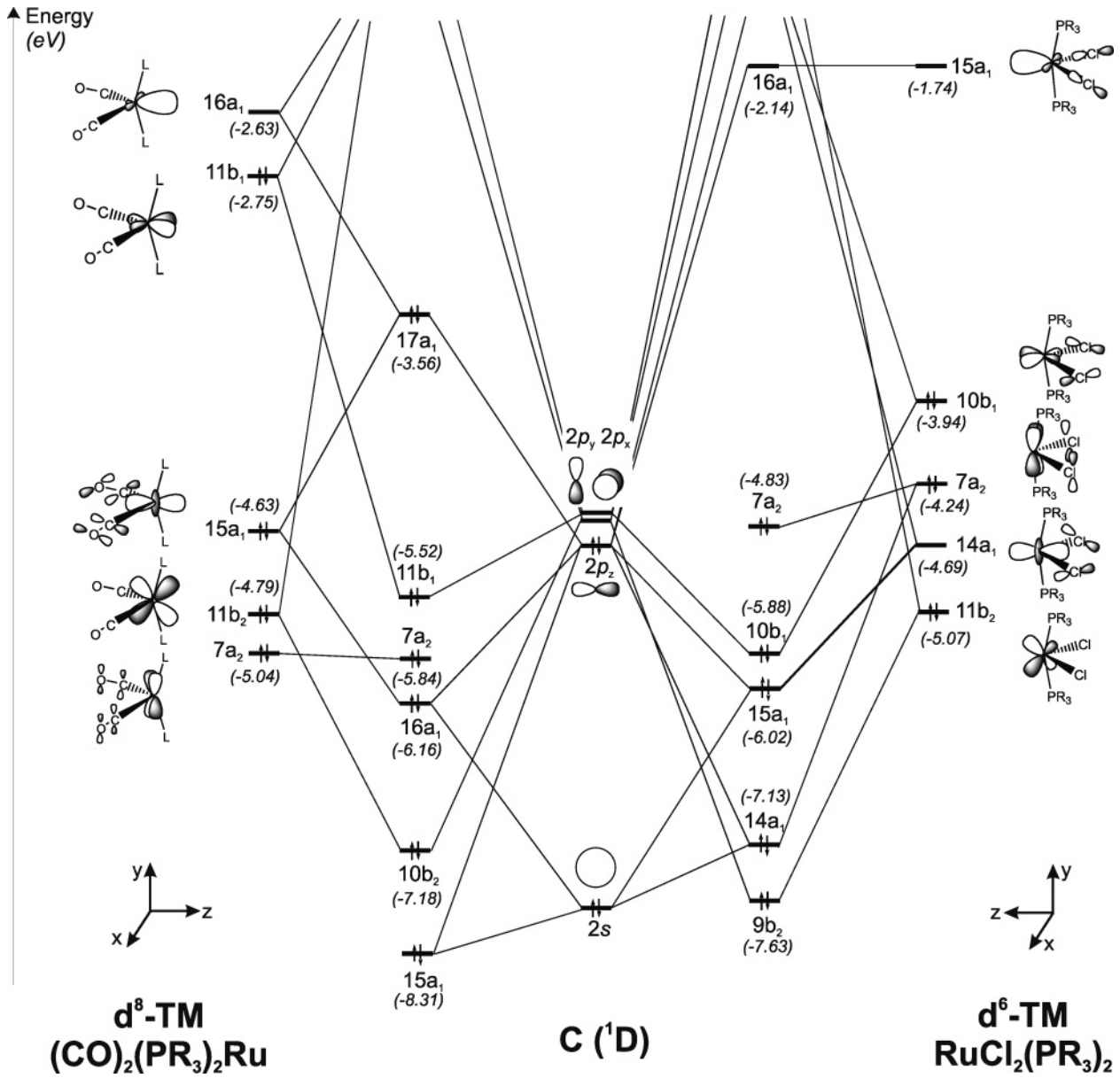

Figure 6. Orbital correlation diagram for the donor−acceptor interactions between a carbon atom with the electron configuration $(2s)^2(2p_\sigma)^2(2p_\pi)^0(2p_\pi)^0$ and the closed-shell TM fragments [$(PMe_3)_2(CO)_2Ru$] (left) and [$(PMe_3)_2Cl_2Ru$] (right). The ordering of the orbitals follows the calculated eigenvalues at BP86/TZ2P shown in Figure 3.

metal−C bonding (Table 5) suggests that the bonding situation in the iron complexes **1Fe**, **2Fe**, and **3Fe-eq** is comparable to the bonding in the corresponding ruthenium compounds (Table 4), but there are also characteristic differences. The absolute values for the $b_2(\pi_\perp)$ orbital contributions are nearly the same for Ru and Fe, but the $b_1(\pi_{||})$ and particularly the $a_1(\sigma)$ terms in the Fe complexes are smaller than those in the Ru complexes. The percentage data indicate that, in the above complexes, iron is a slightly better π donor and significantly weaker σ acceptor than ruthenium.

The larger BDE values of the 18VE iron complexes **2Fe** and **3Fe-eq** than those of the ruthenium analogues **2Ru** and **3Ru-eq** and the trend reversal with respect to the 16VE species **1Fe** and **1Ru** are the result of multiple factors. One factor is the decrease in the preparation energy ΔE_{prep} of the 18VE complexes which is stronger for iron than for ruthenium. More important is the change in the intrinsic interaction energy ΔE_{int} which decreases more strongly for the ruthenium complexes than for the iron compounds. The loss of metal−ligand attraction with respect to **1Fe** or **1Ru** is clearly larger for **2Ru** ($\Delta\Delta E_{int}$ = 60.9 kcal/mol) and **3Ru-eq** ($\Delta\Delta E_{int}$ = 85.8 kcal/mol) than for **2Fe** ($\Delta\Delta E_{int}$ = 41.8 kcal/mol) and **3Fe-eq** ($\Delta\Delta E_{int}$ = 63.7 kcal/mol). It is difficult, however, to single out a particular factor which is responsible for the differences between ruthenium and iron. Inspection of the energy terms shows that for **2TM** the dominant contribution is the change in the Pauli repulsion which decreases much more for **2Fe** ($\Delta\Delta E_{Pauli}$ = 56.7 kcal/mol) than for **2Ru** ($\Delta\Delta E_{Pauli}$ = 38.0 kcal/mol). In the case of **3TM-eq** the situation is less clear-cut where all three energy terms contribute nearly equally to the change in the interaction energy. The changes in the energy terms with respect to **1TM** for the iron complex **3Fe-eq** are $\Delta\Delta E_{Pauli}$ = 83.7 kcal/mol, $\Delta\Delta E_{Elstat}$ = 59.4 kcal/mol, and $\Delta\Delta E_{Orb}$ = 88.0 kcal/mol. The values for the ruthenium complex **3Ru-eq** are $\Delta\Delta E_{Pauli}$ = 77.2 kcal/mol, $\Delta\Delta E_{Elstat}$ = 67.8 kcal/mol, and $\Delta\Delta E_{Orb}$ = 95.2 kcal/mol.

Table 5. Energy Decomposition Analysis at BP86/TZ2P of the Fe−C Bond in the Complexes **1Fe**, **2Fe**, and **3Fe-eq** Using Fragment Pairs A and B as Shown in Figure 4 (Energies in kcal mol^{-1})

	A			B		
	1Fe	**2Fe**	**3Fe-eq**	**1Fe**	**2Fe**	**3Fe-eq**
ΔE_{int}	−221.6	−179.8	−157.9	−145.1	−129.1	−107.9
ΔE_{Pauli}	424.7	368.0	341.0	357.6	378.4	325.2
ΔE_{Elstat}[a]	−339.8 (52.6%)	−306.3 (55.9%)	−280.4 (56.2%)	−232.1 (46.2%)	−246.5 (48.6%)	−209.8 (48.4%)
ΔE_{Orb}[a]	−306.5 (47.4%)	−241.6 (44.1%)	−218.5 (43.8%)	−270.6 (53.8%)	−261.0 (51.4%)	−223.3 (51.6%)
$\Delta a_1(\sigma)$[b]	−115.4 (37.7%)	−77.0 (31.9%)	−90.1 (41.2%)	−115.1 (42.5%)	−136.9 (52.5%)	−121.8 (54.5%)
$\Delta a_2(\delta)$[b]	0.0 (0.0%)	0.1 (−0.1%)	0.0 (0.0%)	−0.2 (0.1%)	0.2 (−0.1%)	−0.2 (0.1%)
$\Delta b_1(\pi_{\|})$[b]	−101.0 (33.0%)	−97.9 (40.5%)	−83.4 (38.1%)	−62.5 (23.1%)	−54.5 (20.9%)	−55.3 (24.8%)
$\Delta b_2(\pi_{\perp})$[b]	−90.1 (29.4%)	−66.8 (27.6%)	−45.0 (20.6%)	−92.8 (34.3%)	−69.8 (26.8%)	−46.0 (20.6%)
ΔE_{Prep}	86.5	64.2	60.0	10.0	13.4	10.0
$-D_e$	−135.1	−115.7	−97.9	−135.1	−115.7	−97.9

[a] The value in parentheses gives the percentage contribution to the total attractive interactions ($\Delta E_{Elstat} + \Delta E_{Orb}$). [b]The value in parentheses gives the percentage contribution to the total orbital interactions.

Table 6. Energy Decomposition Analysis at BP86/TZ2P of the Equatorial TM−CO Bond in **4Ru**, **4Fe**, **5Ru**, **5Fe**, **6Ru**, **6Fe** Using Closed-Shell Fragments (Model A) for the Bonding Analysis (Energies in kcal mol^{-1})

	4Ru	**5Ru**	**6Ru**	**4Fe**	**5Fe**	**6Fe**
ΔE_{int}	−98.1	−52.4	−42.3	−80.5	−63.2	−51.8
ΔE_{Pauli}	211.8	207.2	181.0	183.9	176.1	153.4
ΔE_{Elstat}[a]	−154.5 (49.9%)	−144.6 (55.7%)	−127.3 (57.0%)	−130.0 (49.2%)	−128.7 (53.8%)	−113.5 (55.3%)
ΔE_{Orb}[a]	−155.4 (50.1%)	−115.0 (44.3%)	−96.0 (43.0%)	−134.4 (50.8%)	−110.6 (46.2%)	−91.7 (44.7%)
$\Delta a_1(\sigma)$[b]	−68.5 (44.1%)	−48.8 (42.4%)	−49.5 (51.6%)	−55.1 (41.0%)	−40.3 (36.4%)	−44.0 (48.0%)
$\Delta a_2(\delta)$[b]	−0.1 (0.1%)	0.0 (0.0%)	0.0 (0.0%)	0.0 (0.0%)	0.1 (−0.1%)	0.1 (−0.1%)
$\Delta b_1(\pi_{\|})$[b]	−46.7 (30.1%)	−39.4 (34.3%)	−29.8 (31.0%)	−40.5 (30.1%)	−39.6 (35.8%)	−29.2 (31.8%)
$\Delta b_2(\pi_{\perp})$[b]	−40.1 (25.8%)	−26.8 (23.3%)	−16.7 (17.4%)	−38.8 (28.9%)	−30.8 (27.8%)	−18.6 (20.3%)
ΔE_{Prep}	53.5	12.1	9.8	42.3	8.0	5.5
$-D_e$	−44.6	−40.3	−32.5	−38.2	−55.2	−46.3

[a] The value in parentheses gives the percentage contribution to the total attractive interactions ($\Delta E_{Elstat} + \Delta E_{Orb}$). [b]The value in parentheses gives the percentage contribution to the total orbital interactions.

The EDA results for the metal−carbon complexes **1TM**, **2TM**, and **3TM-eq** shall be compared with the data for the related carbonyl complexes **4TM**, **5TM**, and **6TM** (TM = Ru, Fe) which are given in Table 6. The EDA of the latter species was carried out using bonding model A because it gives the lowest ΔE_{int} values, and thus, it is the appropriate model also for the 16VE complexes **4Ru** and **4Fe**. We first discuss the equatorial bonds.

The equatorial TM−CO bonds are much weaker than the TM−C bonds. This comes from the calculated BDE values and from the ΔE_{int} data. The metal−CO interaction energies ΔE_{int} are between −42.3 and −98.1 kcal/mol, while the metal−C values are between −157.9 and −245.0 kcal/mol. It holds for both ligands that the 16VE complexes have stronger bonds than the 18 VE species. Inspection of the various energy terms which contribute to ΔE_{int} indicate that the natures of the TM−C and TM−CO binding interactions resemble each other. The absolute values for the energy terms which contribute to ΔE_{int} are much larger for the carbon complexes than for the carbonyl complexes, but the relative strengths of the energy terms are not very different from each other. The metal−ligand π backbonding is always slightly stronger than the σ bonding except for **6Ru** where both orbital components have nearly the same strength. The equatorial CO bonds of the complexes **6Ru** and **6Fe** are weaker than those in **5Ru** and **5Fe** (Table 6). The EDA data indicate that this comes mainly from the weaker TM → CO π backdonation in the former compounds. The calculated $\Delta b_1(\pi_{\|})$ and $\Delta b_2(\pi_{\perp})$ values of **6TM** are ∼10 kcal/mol smaller than the analogous data of **5TM**, while the $\Delta a_1(\sigma)$ values change only slightly. The PMe_3 ligands in **5TM** are weaker π acceptors than CO which enhances the TM → CO π backdonation in **5Ru** and **5Fe**. The EDA data in Table 6 nicely support this bonding model.

Table 7. Energy Decomposition Analysis at BP86/TZ2P of the Axial TM−C Bond in **3Ru-ax**, **3Fe-ax** and the Axial TM−CO Bond in **6Ru**, **6Fe** (All Energies in kcal mol^{-1})

	3Ru-ax	**3Fe-ax**	**6Ru**	**6Fe**
fragments	A	A	A	A
ΔE_{int}	−203.1	−168.7	−53.3	−55.4
ΔE_{Pauli}	439.3	341.0	132.5	136.7
ΔE_{Elstat}[a]	−362.3 (56.4%)	−280.3 (55.0%)	−98.9 (53.2%)	−99.2 (51.6%)
ΔE_{Orb}[a]	−280.1 (43.6%)	−229.4 (45.0%)	−86.9 (46.8%)	−92.9 (48.4%)
$\Delta a_1(\sigma)$[b]	−126.8 (45.3%)	−103.0 (44.9%)	−45.4 (52.2%)	−47.7 (51.3%)
$\Delta a_2(\delta)$[b]	0.0 (0.0%)	0.0 (0.0%)	0.0 (0.0%)	0.0 (0.0%)
$\Delta e(\pi)$[b]	−153.3 (54.7%)	−126.4 (55.1%)	−41.5 (47.8%)	−45.2 (48.7%)
ΔE_{Prep}	114.3	64.2	20.8	9.1
$-D_e$	−88.8	−104.5	−32.5	−46.3

[a] The value in parentheses gives the percentage contribution to the total attractive interactions ($\Delta E_{Elstat} + \Delta E_{Orb}$). [b]The value in parentheses gives the percentage contribution to the total orbital interactions.

We also analyzed the metal−carbon bonding in the more stable axial isomers **3Ru-ax** and **3Fe-ax** and compared the EDA results with the data for the axial TM−CO bonds in **6Ru** and **6Fe**. The results are given in Table 7.

The axial Ru−C bond in **3Ru-ax** has a much higher interaction energy (ΔE_{int} = −203.1 kcal/mol) than the equatorial Ru−C bond in **3Ru-eq** (ΔE_{int} = −159.2 kcal/mol), while the interaction energy for the Fe−C bond in **3Fe-ax** (ΔE_{int} = −168.7 kcal/mol) is only slightly higher than that for the equatorial Fe−C bond in **3Fe-eq** (ΔE_{int} = −157.9 kcal/mol). This is in agreement with the difference between the equatorial and axial metal−C distances (Figure 1). The Ru−C bond length

in **3Ru-ax** (1.706 Å) is much shorter than the equatorial Ru−C bond in **3Ru-eq** (1.784 Å), while the axial Fe−C distance in **3Fe-ax** (1.641 Å) is less shortened with respect to the equatorial Fe−C bond in **3Fe-eq** (1.675 Å). The calculated data prove once again that the intrinsic interaction energy between the actual fragments in a molecule is a much better probe for the strength of the binding interactions than the bond dissociation energy. The BDE value of **3Ru-ax** (D_e = 88.8 kcal/mol) is only slightly higher than the BDE value of **3Ru-eq** (D_e = 83.7 kcal/mol), while the difference between the BDE values of the axial isomer **3Fe-ax** (D_e = 104.5 kcal/mol) and the equatorial form **3Fe-eq** (D_e = 97.9 kcal/mol) is even higher than that for the ruthenium species. Note that the ruthenium complex **3Ru-ax** has a much higher metal−C interaction energy than the iron complex **3Fe-ax**, but the BDE value of the latter is clearly higher than that for the former. The carbon ligand in **3Ru-ax** is intrinsically more strongly bonded than that in **3Fe-ax**, although the iron complex has a higher bond dissociation energy.

A comparison of the EDA results for the 16VE and 18VE complexes with a carbon atom and CO ligands shows that there is no single factor which explains why the ruthenium−ligand bonds of the 16VE species have larger bond dissociation energies than the iron−ligand bonds while the opposite trend is predicted for the 18VE compounds. This becomes obvious when the results for the carbon complexes **1TM** (16VE) and **2TM** (18VE) using model A are compared with the data for **4TM** (16VE) and **5TM** (18VE). For the carbon complexes, the weakening of the attractive terms $\Delta E_{elstat} + \Delta E_{orb}$ when one goes from **1Ru** to **2Ru** (98.9 kcal/mol) is nearly the same as that for the iron complexes **1Fe** to **2Fe** (98.5 kcal/mol; see Tables 4 and 5). The relatively stronger bond of the iron complexes comes from the stronger reduction of the Pauli repulsion ΔE_{Pauli} between **1Fe** and **2Fe** (56.7 kcal/mol) compared with **1Ru** and **2Ru** (38.0 kcal/mol). In the case of the carbonyl complexes we find that the attractive terms $\Delta E_{elstat} + \Delta E_{orb}$ are the crucial factor which yields a stronger bond for Fe−CO than for Ru−CO in the 18VE complexes. The latter terms decrease from **4Ru** to **5Ru** by 50.2 kcal/mol, while the lowering from **4Fe** to **5Fe** is only 25.1 kcal/mol. The decrease of the Pauli repulsion in the former ruthenium complexes (4.5 kcal/mol) is even slightly less than that in the latter iron species (7.7 kcal/mol). But for all complexes it holds that the 18 VE compounds have longer and weaker TM−C and TM−CO bonds than the respective 16 VE compounds. This is because the LUMO in the 16VE species is a σ-antibonding orbital which becomes occupied in the 18VE species. Figure 5 shows that the shape of the LUMO of **4Ru** in the Ru−CO bonding region looks very similar to the LUMO of **1Ru** in the Ru−C area (Figure 3). Likewise the HOMO of **2Ru** and the a_1 component of the degenerate HOMO 10e′ of **5Ru** possess a similar shape in the Ru−ligand region (Figure 5).

Summary and Conclusion

The calculations which are presented in this paper show that the ruthenium−carbon bond in the 16VE complex $[Cl_2(PMe_3)_2Ru(C)]$ (**1Ru**) which serves as model compound for the recently synthesized species $[(PCy_3)_2Cl_2Ru(C)]$ is very strong. The theoretically predicted BDE of **1Ru** is D_e = 146.5 kcal/mol. This is much higher than the BDE of the related CO complex $[Cl_2(PMe_3)_2Ru(CO)]$ (**4Ru**) which has a BDE of D_e = 44.6 kcal/mol. The analogous iron complex $[Cl_2(PMe_3)_2Fe(C)]$ (**1Fe**) is more weakly bonded (D_e = 135.1 kcal/mol) than **1Ru**. The 18VE complexes $[(CO)_2(PMe_3)_2Ru(C)]$ (**2Ru**), $[(CO)_2(PMe_3)_2Fe(C)]$ (**2Fe**), $[(CO)_4Ru(C)]$ (**3Ru**), and $[(CO)_4Fe(C)]$ (**3Fe**) have less strongly bonded C ligands than **1Ru** and **1Fe**. The 16VE ruthenium complexes have larger bond dissociation energies for the C and CO ligands than the 16VE iron complexes. The opposite trend is calculated for the 18VE complexes. Here, the iron complexes have a higher BDE than the ruthenium compounds.

Energy decomposition analysis of the metal−C bonds in **1Ru**−**3Fe** and comparison with the related metal−CO bonds in the complexes $[(PMe_3)_2Cl_2Ru(CO)]$ (**4Ru**), $[(PMe_3)_2Cl_2Fe(CO)]$ (**4Fe**), $[(PMe_3)_2Ru(CO)_3]$ (**5Ru**), $[(PMe_3)_2Fe(CO)_3]$ (**5Fe**), $[Ru(CO)_5]$ (**6Ru**), and $[Fe(CO)_5]$ (**6Fe**) show that the intrinsic interaction energies between the frozen metal fragments and the ligands is a better probe for the understanding of the bonding situation than the bond dissociation energies. The Ru−C and Fe−C bonds in **1Ru** and **1Fe** are best described in terms of interactions between a carbon atom with the electron configuration $(2s)^2(2p_{z(\sigma)})^1(2p_{x(\pi)})^1(2p_{y(\pi)})^0$ and a metal fragment with the corresponding electron configuration at the metal atom $d_z2(\sigma)^1d_{xz}(\pi)^1d_{yz}(\pi)^2$. This yields two electron-sharing bonds with σ and π symmetry and one donor−acceptor π bond. Charge and energy decomposition analyses suggest that the stronger TM−C bond in the 16VE complexes **1Ru** and **1Fe** compared to the 18VE analogues comes mainly from enhanced metal−C σ interactions. This seems to be the pivotal reason that the 16VE complexes **I** and **II** are stable enough to become isolated. The bonding situation in the 18VE complexes **2Ru**−**3Fe** is better described in terms of closed-shell donor−acceptor interactions between a carbon atom possessing the electron configuration $(2s)^2(2p_{z(\sigma)})^2(2p_{x(\pi)})^0(2p_{y(\pi)})^0$ and metal fragments with the configuration $d_z2(\sigma)^0d_{xz}(\pi)^2d_{yz}(\pi)^2$. Inspection of the various energy terms which contribute to ΔE_{int} indicates that the natures of the TM−C and TM−CO binding interactions resemble each other. The absolute values for the energy terms which contribute to ΔE_{int} are much larger for the carbon complexes than those for the carbonyl complexes, but the relative strengths of the energy terms are not very different from each other. The π bonding contribution to the orbital interactions in the carbon complexes is always stronger than σ bonding. There is no particular bonding component which is responsible for the reversal of the relative bond dissociation energies of the Ru and Fe complexes when one goes from the 16VE complexes to the 18VE species. For all complexes it holds that the 18VE compounds have longer and weaker TM−C and TM−CO bonds than the respective 16VE compounds. This is because the LUMO in the 16VE species is a σ antibonding orbital which becomes occupied in the 18VE species.

Acknowledgment. We thank one referee for very helpful comments. This work was supported by the Deutsche Forschungsgemeinschaft. Excellent service by the Hochschulrechenzentrum of the Philipps-Universität Marburg is gratefully acknowledged. Further computer time was provided by the HHLRZ Darmstadt.

Supporting Information Available: Complete refs 51 and 53. Cartesian coordinates (in Å) and total energies of all compounds discussed in the text. This material is available free of charge via the Internet at http://pubs.acs.org.

JA0691324